Rheinisch- Westfälische Technische Hochschule Aachen
Fakultät für Georessourcen und Materialtechnik
Lehr- und Forschungsgebiet Geologie – Endogene Dynamik

Capturing a world-class outcrop of a quality calcite vein network on a polished limestone outcrop in the Oman Mountains: Creation of a high resolution panorama and microstructural vein description

B.Sc.-Thesis

Patrick Wüstefeld

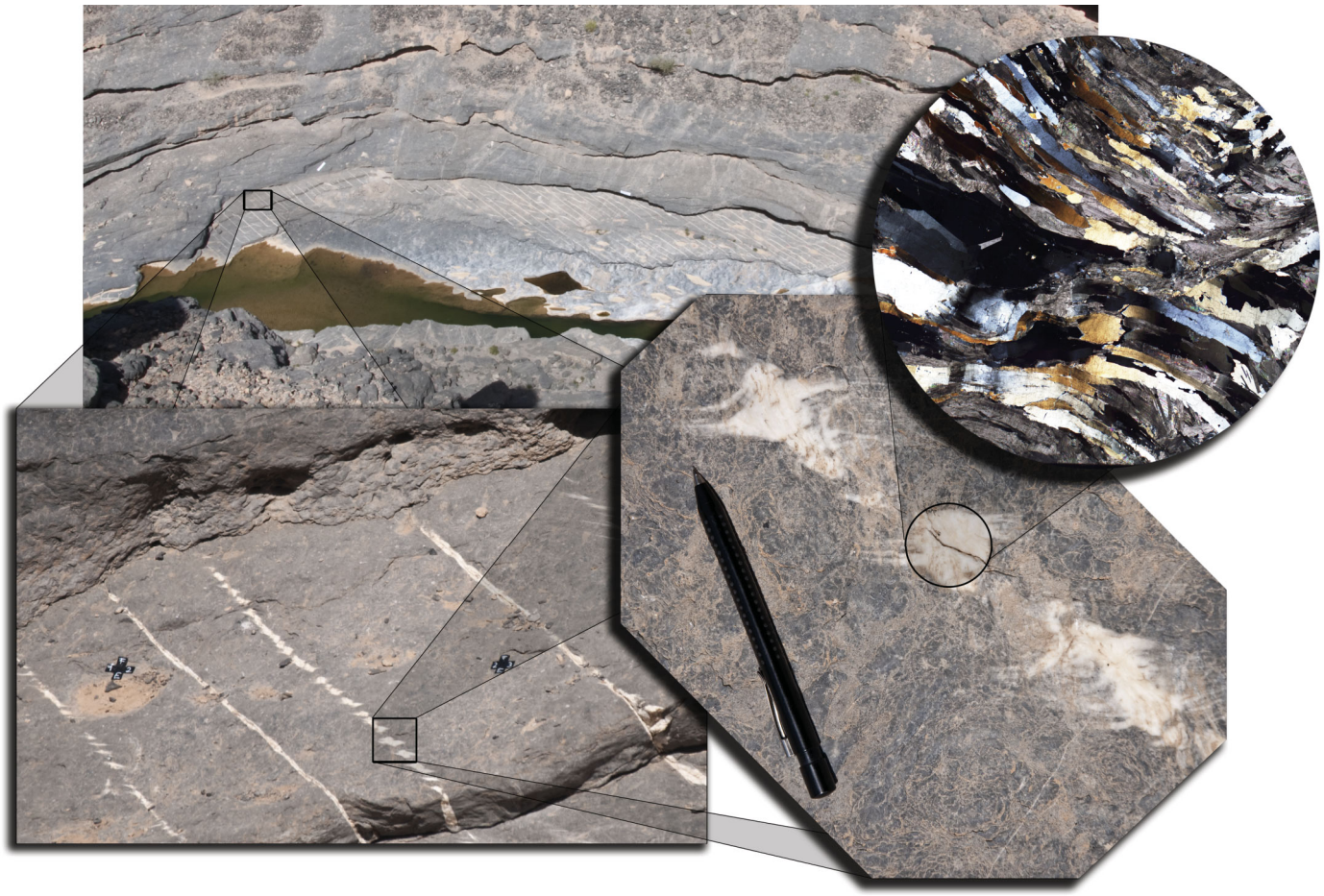

Supervisor:
Prof. Dr. Janos L. Urai

communicated by **Prof. Dr. J.L. Urai**

LuF für Geologie – Endogene Dynamik
Structural Geology, Tectonics and Geomechanics
Lochnerstrasse 4-20
52056 Aachen
www.ged.rwth-aachen.de

Bachelor Thesis eingereicht am 13. Oktober 2010 durch Patrick Wüstefeld.

Hiermit erkläre ich an Eides statt, dass ich die von mir vorgelegte Arbeit selbstständig verfasst habe, dass ich keine weiteren Hilfsmittel als die angegebenen benutzt habe.

Aachen, den 13. Oktober 2010

_____

Patrick Wüstefeld

Abstract

We studied a high quality calcite vein network on a polished limestone outcrop in the Oman Mountains. In most cases outcrops of scientific interest are situated far away and therefore only reachable for a certain time period. The Oman Mountains provide a huge amount of world-class outcrops. The aim of this work is to create a high-resolution panorama of an outcrop called 'the Swimming Pool Pavement', which is situated in Wadi Dham at the southern slope of Jabal Sarrah. The outcrop consists of a high-quality calcite vein network on a polished limestone outcrop (Natih Formation). We found three different vein sets in the pavement. The outcrop panorama allows several further office-based investigations and therefore is a powerful tool. The thesis describes methodology and workflow of the panorama generation, compares different approaches of image acquisition and evaluates different important parameters that influence image stitching accuracy. Integrated detail pictures taken at spots of interest and calcite vein thin section images allow to work on different scales: one can zoom into the panorama from bird's eye view to microscopic scale. Field observations and microstructural description of fibrous calcite veins (set 1) give a first approach to the structural geology of the outcrop.

Contents

1 Introduction

The Oman Mountains offer a huge amount of world-class outcrops with remarkable conditions for geological surveys, “exposure is frequently 100% with little soil or vegetation coverage” (cit. Searle 1985). The principal aim of the bachelor research is the creation of high resolution panoramas of calcite vein networks on polished, Mesozoic limestone outcrops. The thesis describes methodology and workflow of the panorama generation, compares different approaches of image acquisition and evaluates different important parameters that influence image-stitching accuracy. Generating detailed panoramas of outcrops offers the possibility for further office-based investigations and therefore is a powerful tool. This could be an interesting addition to conventional fieldwork for similar projects in the future. In addition to the panorama generation, this thesis basically describes the vein network of the outcrop and includes an elementary microstructural vein description of a certain set of veins. The duration of the fieldwork in Oman was 6 weeks, namely from 22nd February until 31st March 2010.

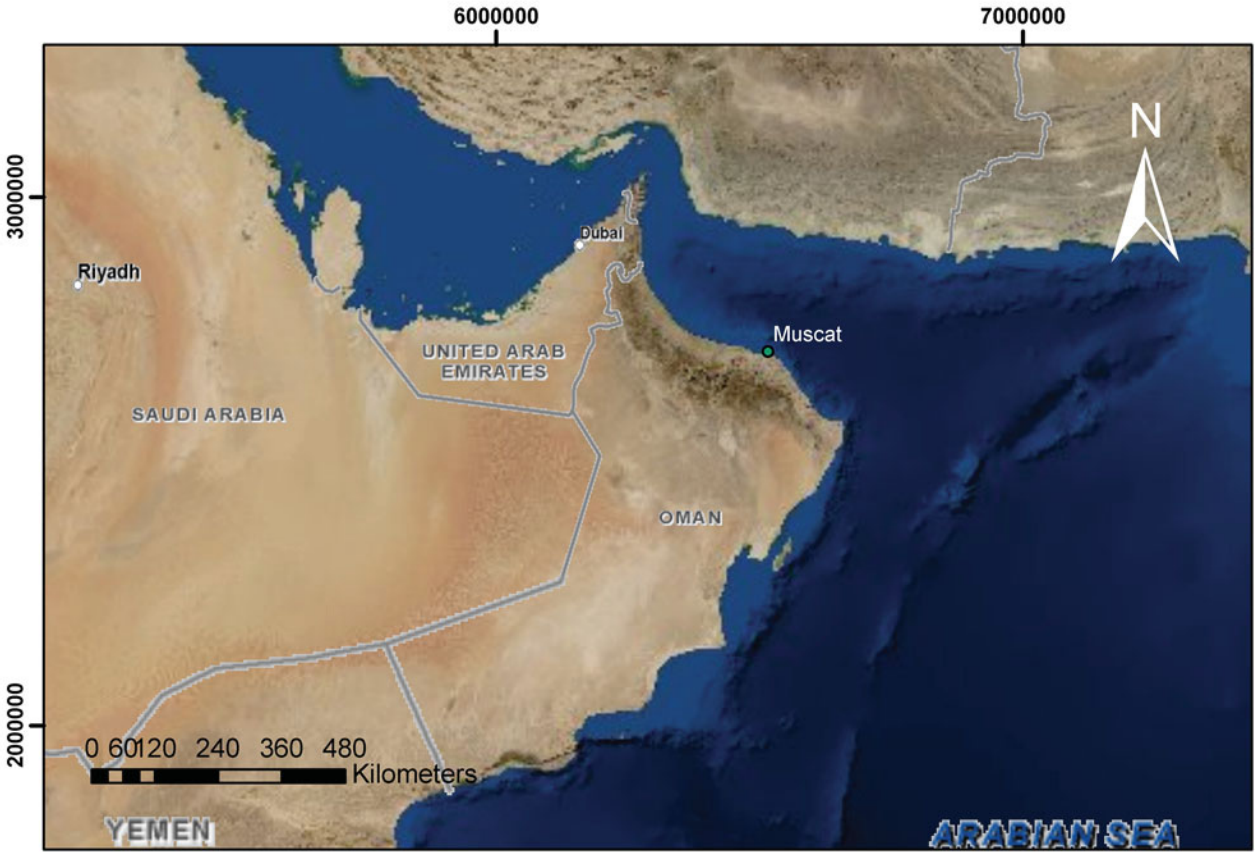

Fig. 1: Landsat image showing the eastern Arabian Peninsula with the Sultanate of Oman in the centre. The Oman Mountains in the N of Oman are well visible. Bordering countries are the United Arab Emirates, Yemen and Saudi Arabia. (GCS_WGS_1984 coordinate system)

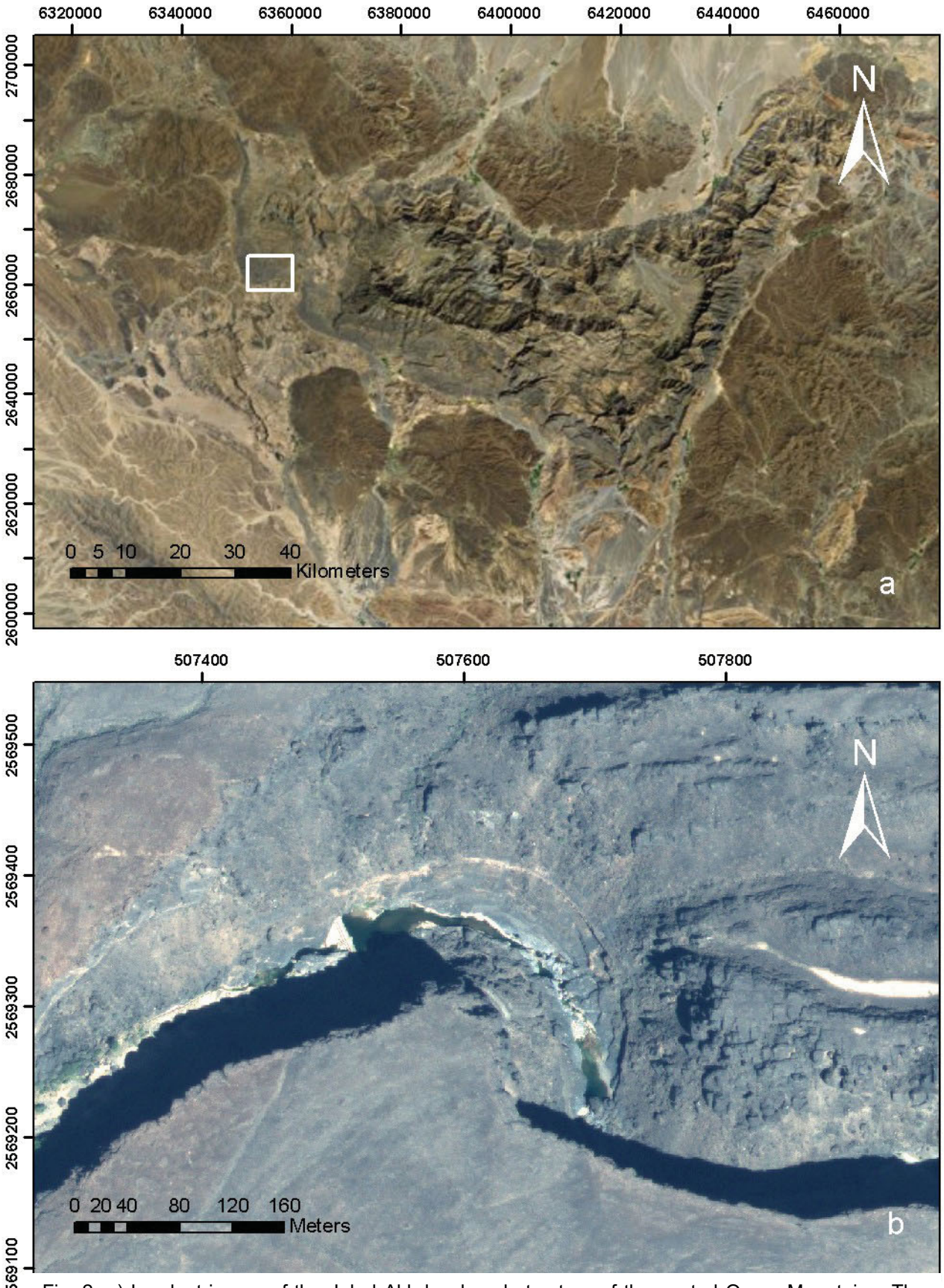

Fig. 2: a) Landsat image of the Jabal Akhdar domal structure of the central Oman Mountains. The white rectangle marks the southern slope of Jabal Sarrah, where the working area (image b) is located. (GCS_WGS_1984 coordinate system)
b) GeoEye image of the Swimming Pool pavement, which is located in Wadi Dham at the southern slope of Jabal Sarrah. (UTM 40Q)

1.1 Study area

The study area is situated in Wadi Dham; at the southern slope of Jabal Sarrah, which is still part of the Jabal Akhdar domal structure (Fig. 2.) It is reachable from the village Barut. The GPS coordinates of the outcrop are 2569404 m N 507637 m E (UTM 40 Q). The outcrop's dimensions are roughly 90m in EW-direction and 12 m in NS-direction.

1.2 Geological outline

The Oman Mountains are situated in the NE of the Arabic peninsula (Fig. 1), with the NW end at the Musandam peninsula and the SE end at the Batain coast (Holland 2009). They are "part of the Alpine-Himalayan chain" (cit. Holland 2009). The basis for the formation of the orogen took place at the beginning of upper cretaceous, roughly more than 90 Ma ago: primary the crust of the Neo-Tethys was subducted into an intra-oceanic subduction zone, followed by the Arabian continental margin, which eventually subducted under the oceanic plate; a process called obduction (Glennie 1995, Holland 2009). This caused the emplacement of the allochtonous over the autochtonous units. A famous example of the allochtonous units is the Semail Ophiolite, "which consists mainly of a slab of former oceanic crust" (cit. Glennie 1995). "The timing of uplift and folding of this part of the Oman Mountains is unclear and subject to a debate"(cit. Holland 2009), Glennie (1995) for example proposes tertiary age.

The important formation for this work is part of the autochtonous unit B, also known as Hajar Supergroup (Glennie 1995), which was deposited on the passive margin of the Arabian plate (Holland 2009, Glennie 1995). The Hajar supergroup consists mostly of carbonates; rich in carbonate fragments (Glennie 1995). The Wasia group, which is one of the youngest groups of the Hajar supergroup, "was deposited in shallow water conditions of a subtidal environment" (cit. Holland 2009). The studied limestone outcrop belongs to the Natih formation, the youngest strata of the Wasia group. It consists of "argillaceous wackestone, bioclastic packstone and grain stone" (cit. Holland 2009, Pratt 1993).

2 Material and Methods

2.1 Fieldwork Oman

2.1.1 Logistics

2.1.1.1 Vehicles

In order to be able to work in the Oman Mountains, an off-road capable car is indispensable. Two 4-wheel-drive jeeps with PDO[1] specifications were rented for the group. These specifications are to be strongly recommended as they upgrade usual security standards.

2.1.1.2 Equipment

Basic equipment as for example camping equipment is provided by the German University of Technology, as is the core-drilling machine (cp. chapter 2.1.6). Further equipment – e.g. compasses, cameras, etc. – has to be imported from Germany or be purchased in Muscat. It is almost impossible to acquire special equipment outside of the Muscat capital area as for example in towns like Nizwa.

As the working areas are not easy to access, it should be kept in mind that equipment has to be carried to the working areas over difficult terrain. A well-organized plan as to what is required for each working day is therefore essential.

2.1.1.3 Accommodation

Camping is a cheap alternative in Oman, as there are no restrictions. A camping site near the working area allows for an early working start in the morning. This is favourable for work within a certain time frame or for working before noon in order to avoid extremely high temperatures.

The second alternative is renting a house, which is possible at a relatively low cost. A house for the group was rented in Al Hamra. The advantages are a more comfortable lifestyle – e.g. toilette, kitchen etc. – and a storage facility. The disadvantage is the distance to the working area.

[1] Petroleum Development Oman

Fig. 3: Bird's eye view of the swimming pool pavement shot from spot 2. The red line marks the shape of the outcrop.

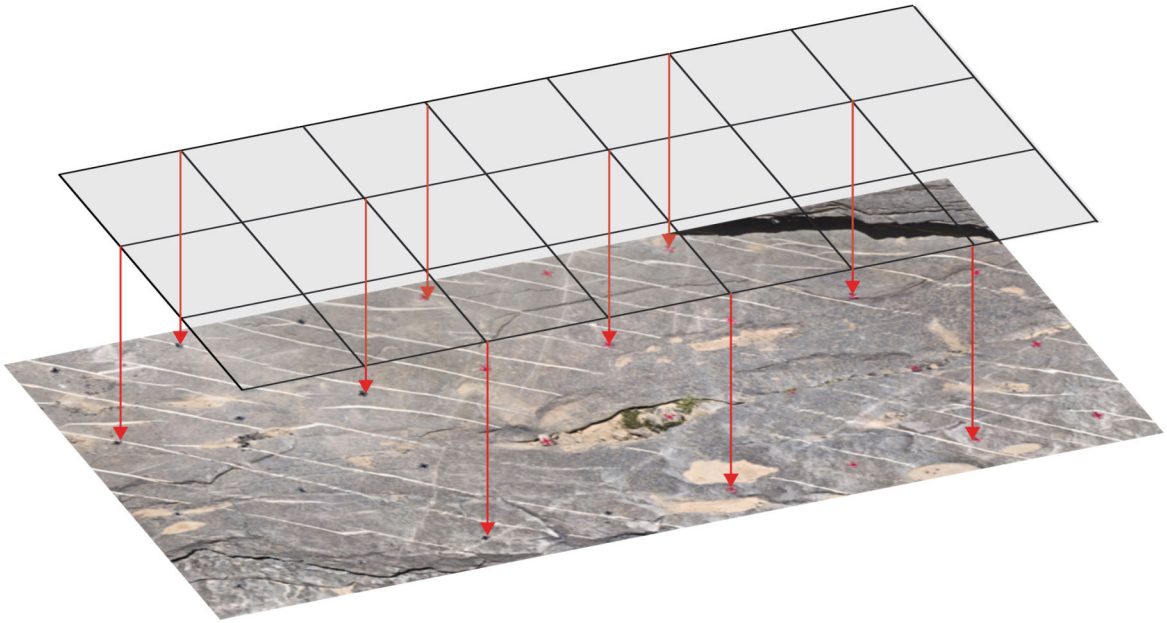

Fig. 4: Scheme illustrating the gridding process. The imaginary plane lies over the pavement. The grid points are projected perpendicular onto the pavement.

2.1.2 Gridding of the pavement

A grid on the pavement is essential for further scientific work with the panorama. Apart from this purpose, the grid is needed for the rectification of the pavement (cp. chapter 2.2.1.3).
To obtain the grid, an imaginary flat plane is assumed to lie over the pavement (cp. Fig. 4). The grid points are projected perpendicular from this plane onto the pavement. To define the imaginary plane it is preferable to use the dip and dip direction of the pavement's layers itself because they seem to be approximately homogeneous. This technique is used because the aim is to finally obtain a perpendicular view onto the pavement reached by the rectification. The favoured grid size are quadrants with 2m edge length.

2.1.2.1 Projecting stick

To project the points onto the pavement a self-made 'projecting stick' is invented (Fig. 5). In order to achieve this, a broomstick is combined with two spirit levels and a measuring tape. This tool ensures the orthogonality of the projection onto the imaginary plane. The spirit levels are fixed to the broomstick with a hinge, which can be adjusted with the dip of the imaginary plane. The rotation of the broomstick around its own axis is a parameter, which must be controlled by a compass and would otherwise affect the dip direction of the broomstick. The measuring tape attached to the broomstick enables the distance between each grid point and the imaginary plane to be recorded.

Fig. 5: Working with the projecting stick: The tool ensures the orthogonality of the projection onto the pavement. The grid points are primary marked with a permanent marker on the pavement. Strings and a measuring tape span the imaginary plane over the pavement (not visible in the picture).

2.1.2.2 Creating the Grid

The pavement is measured at several spots to obtain an averaged value for dip direction and dip: 221°/9° (cp. A. 10). For the practical realization, the imaginary plane will have a slight deviation because of the limited possibilities to span the grid, as explained in the following.

The skeletal structures of the gridding are two strings spanned over the pavement, parallel to each other. The first string is fixed by a stone in the east and a tripod in the west. The second string is fixed by two stones. An amplitude compass controls the orientation of both axes and additionally the parallelism is checked by measuring the distance between the two axes at distal control points. The measured orientation are 290°/2° for the first axis and 290°/3,5° for the second axis which is acceptable for the set up. In order to calculate the resulting imaginary plane, the height difference between both axes is measured as the dip of a connecting linear which is perpendicular to the axes, measured twice on distal control points. With this information - visualized in Fig. 6 - the orientation of the effective imaginary plane is 222°/06° (dip direction/dip), which is a good approach to the favoured imaginary plane defined by the measured dip direction and dip of the pavement.

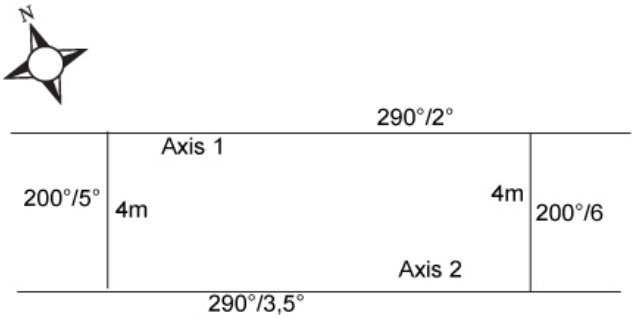

Fig. 6: Schematic illustration of the spanned imaginary plane. Both main axes are present as well as the connecting lines to calculate the effective imaginary plane. Dip directions and dips mark lines.

Beginning in the west both axes are marked with a permanent marker every two meters, ensuring that the connection line between two corresponding marks is perpendicular to the axes. A measuring tape is spanned perpendicular to both main axes. Two corresponding marks (previously mentioned) on the main axis define the orientation of the measuring tape according to a linear described by two points. Beginning with the mark on the first axis and following the measuring tape (linear) along in intervals of two meters the points are marked on the pavement with permanent marker using the projecting stick (cp. Fig. 5). After projecting the first row of points the measuring tape is moved to the next corresponding set of marks on the main axes and the procedure is repeated with each set of corresponding marks. A third main axis parallel to the first ones has to be spanned to cover the whole pavement; the technique of projecting remains the same. Additionally the distances of the grid points to the imaginary plane are recorded.

Fig. 7: Preparing the pavement for imaging: spots of interest have to be cleaned.

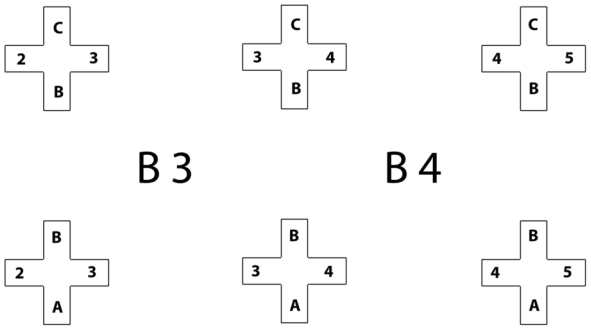

Fig. 8: Scheme illustrating the nomenclature of the grid.

2.1.2.3 Preparing the grid and pavement for imaging

The grid has to be prepared for imaging. This involves taping over the grid points already marked with permanent marker with a well visible cross, made of adhesive foil. Thus ensuring the visibility of the grid points in the images. The grid points receive a numeration to identify the quadrants using the scheme shown in Fig. 8.

In addition a rough cleansing of the pavement must be carried out. As the location is popular with tourists, littering of the swimming pool pavement is common. Before imaging can take place, this rubbish has to be removed. Rocks, mud or the like which cover interesting parts of the pavement should be removed as well.

2.1.3 Imaging from fixed spots

2.1.3.1 Equipment

The camera used for imaging is a Nikon D90, combined with a Sigma 120.0-400.0mm f/4.5-5.6 lens. As the sensor dimension of the camera is 23,6 mm x 15,8 mm, a crop factor of 1,5 has to be used to obtain the effective maximal focal length of 600 mm (to keep it simple, in the following the crop factor won't be considered, i.e. the maximal focal length for this objective will remain 400 mm). A Manfrotto Tripod with three adjustable axes is used to set up the camera.

2.1.3.2 Selecting the spot

In order to select the spot two main requirements have to be regarded:

- Distance
- Orthogonality

The distance from the imaging spot to the pavement is an important aspect concerning the resolution of the final image. The orthogonality affects the view onto the pavement and this

results in a perspective distortion of the image. Further important is the limited availability of spots and the security aspects.

Taking these circumstances into account, two different imaging spots are chosen as described in the following chapters.

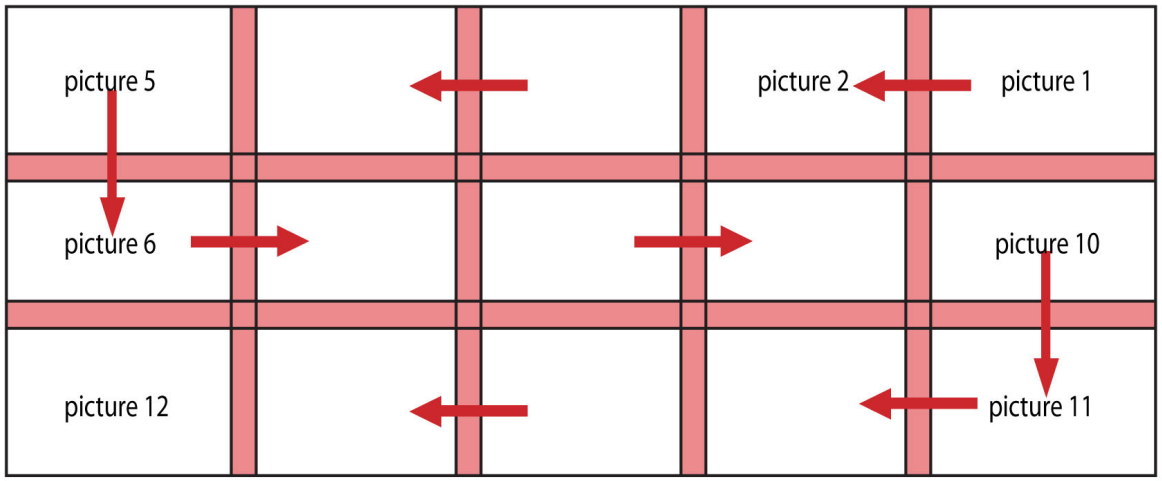

Fig. 9: Scheme of imaging the outcrop systematically. The red areas represent the overlapping of the images.

Fig. 10: Image acquisition from fixed spot 2.

2.1.3.3 The technique of imaging

The aim of imaging is to obtain a series of pictures which can be stitched together afterwards using a computer. It is therefore of extreme importance to take pictures, which overlap other neighbouring pictures. To be able to ensure for this, the pavement is photographed systematically in rows and the photographer has to assure that one site of the picture overlaps with the next picture (cp. Fig. 9). An overlap of roughly 1/10 of the horizontal length of the image sector is used. The tripod used has three adjustable axes so it is very easy to follow the rows by just using the horizontal axis. Once a row is completed, another row can be focussed by adjusting the vertical axis, ensuring once again for an overlap of the pictures. The overlap used in vertical direction is roughly 1/7 of the vertical length of the image sector. This way the entire pavement can be easily and systematically rasterised by images. Each picture is taken with two seconds retardation to prevent camera shaking caused by handling the camera.

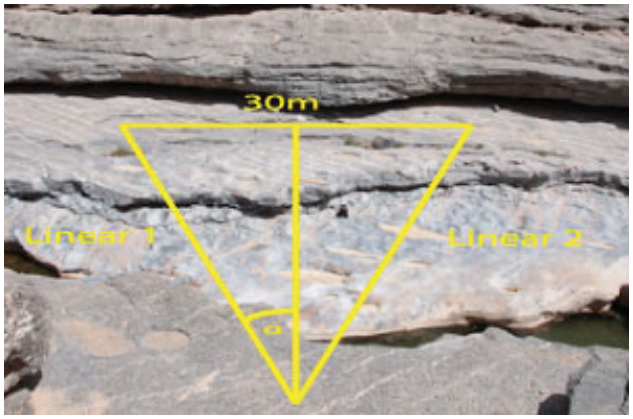

Fig. 11: Scheme illustrating the basis for distance and viewing angle estimation (averages). **Spot 1** has the measured data 013°/36° for linear 1 and 044°/36° for linear 2. This delivers an angle alpha of 15,5°. With trigonometrically relationships a distance of 55 m is calculated. According to this, for **Spot 2** (measured: 001°/48° and 016°/48°) results a distance of 114 m. The lines define a plane (yellow triangle), which cuts the imaginary plane. The angle between both planes defines the averaged viewing angle.

2.1.3.4 Spot 1

The GPS data of this spot is 2569376 m N and 507620 m E (UTM 40Q). The distance to the pavement is roughly 55 m, which is calculated by locating two points with known distance (cp. Fig. 11). Additionally an averaged viewing angle of 43° to the imaginary plane is derived from this data (cp. Fig. 11). It has to be kept in mind that this angle of course varies for each location of the pavement; it just should give an idea of the viewing angle.

2.1.3.5 Spot 2

The GPS data of the second Spot is 2569366 m N 507610 m E (UTM 40Q). The calculated distance is roughly 114 m, analogue to the calculation used for Spot 1 (cp. Fig. 11). The averaged viewing angle is 53°.

2.1.3.6 Series of fixed spot image acquisition

From each spot different series with different focal lengths are taken:

- Series 1, Spot 1, 400 mm: 213 images
- Series 2, Spot 1, 200 mm: 58 images
- Series 3, Spot 1, 120 mm: 23 images
- Series 4, Spot 2, 400 mm: 84 images
- Series 5, Spot 2, 200 mm: 21 images

The aim of this procedure is to find out if it is necessary to use the maximal focal length available. A smaller focal length would save time, as fewer pictures would be taken. This is topic of chapter 3.1.1.1.(a).

2.1.4 Imaging with the dipod

A further method used for photographing the pavement surface is carried out using the dipod construction. The main difference is the absence of a fixed imaging spot. Simon Virgo and Max Arndt used the technique in their diploma work (Virgo & Arndt 2010).

Fig. 12: Imaging with the dipod. The dipod setup is well visible: two expandable aluminium rods and the camera fixed at the aluminium traverse. The picture shows Simon Virgo and Max Arndt using the dipod to image a pavement as part of their diploma work. (picture: Virgo and Arndt 2010)

2.1.4.1 Dipod setup

The dipod (cp. Fig. 12) used for imaging, basically consists “of two expandable telescopic aluminium rods (originally sold as gardening tools) and a custom-made aluminium traverse that can carry a digital camera via a quick release plate” (cit. Virgo & Arndt 2010). The Dipod enables pictures to be taken vertically onto the outcrop surface. It has to be handled by two people; spirit levels guarantee the correct alignment of the construction (Virgo and Arndt 2010). “The Telescopic legs can be locked in 4 positions, allowing shots from the heights of 1,57 m; 1,85 m; 2,3 m; 2,6 m” (cit. Virgo and Arndt 2010). The camera, which is used for the setup is a Nikon D 80 combined with a Tokina AT-X 4,0/12-24 mm Pro lens.

2.1.4.2 Imaging with the dipod

The aim of imaging with the dipod technique is to be able to compare both techniques afterwards. Just the eastern part of the outcrop surface is therefore imaged with the dipod. “The photographs were taken by stepwise carrying the dipod”(cit. Virgo & Arndt 2010) along traverses defined by the E-W oriented principal grid axis. As is the case for the imaging technique from a fixed imaging spot, it is essential for the dipod technique to guarantee the overlapping of single images. For further information on the image acquisition read Virgo & Arndt (2010).

2.1.5 Detail work

In addition to the main project – the acquisition of image data – detailed work on the pavement forms the second part of this bachelors’ thesis. This includes basic information of the vein structure of the pavement. For an efficient data acquisition of the pavement, an attribute checklist is used for each analyzed vein (cp. A. 9).

Fig. 13: Both pictures show the same spot, taken with different camera orientations. Picture a is shot in **PV** whereas picture b is shot in **MV**. 2 veins of set 1 are connected by a step over. The structure is exposed in 3D, located at the border of layer I & 2 in quadrant D 1. Due to the viewing orientation and 3D effects the aperture of the step over appears too big in picture a. In picture b the veins don’t appear entirely straight; again an effect of topography with a certain viewing orientation.

2.1.5.1 Detail pictures

The pictures are a secondary visual documentation of the analyzed veins. The camera used for the detail pictures is a Nikon D90 combined with a Nikon standard lens, AF-S DX VR 18-105mm f/3,5-5,6.

Three main camera orientations are defined:

- **MV = map view**
- **PV = profile view**
- **SV = side view**

The map view orientation (cp. Fig. 13b) is perpendicular to the bedding, the profile view (cp. Fig. 13a) is perpendicular to the plane defined by dip direction and dip of the vein, the side view orientation is parallel to the bedding and parallel to the strike direction of the vein.

An additional aim of the map view pictures is the integration to the final panorama. This will allow a higher resolution at points of interest.

2.1.5.1.(a) Age relationships

Spots with clear age relationships are photographed to integrate them as well into the final high resolution panorama. A nomenclature is used to visualize the age relationships: one point marking the youngest vein; two points marking the older vein; etc. (cp. Fig. 14).

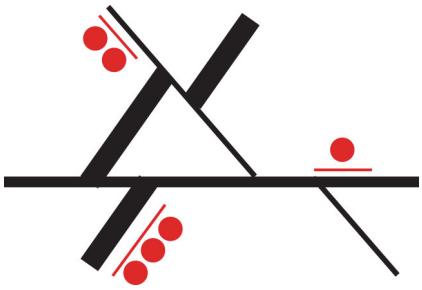

Fig. 14: Sketch of age relationship nomenclature.

Fig. 15: Drilling plugs out of vein set 1 using a CARAT hands-free core drilling machine type 2011.

2.1.6 Samples

Apart from the in situ data acquisition, samples are taken to prepare thin sections. As vein structure is of capital interest, it is favourable to get samples directly out of the vein. A core-drilling machine is used to drill 'plugs' (cores with calibre of 35 mm and a rough length of 10 cm) out of vein set 1 (cp. chapter 3.3.1).

2.1.6.1 Equipment

The core-drilling machine, which is used, is a CARAT hands-free core drilling machine type 2011 (cp. Fig. 15), combined with a diamante core drill of 35 mm calibre. A mobile manual pump provides the core driller with cooling water. The logistic for the water is simple because the Wadi is water bearing. A mobile Honda power generator provides electricity.

2.1.6.2 Plug orientation

For the plugs four drilling directions are predefined, which are supposed to be useful for further investigations. The scheme seen in Fig. 16 illustrates the four principal orientations:

- **X**-orientation
- **Y-**orientation
- **Z**-orientation
- **g**-orientation

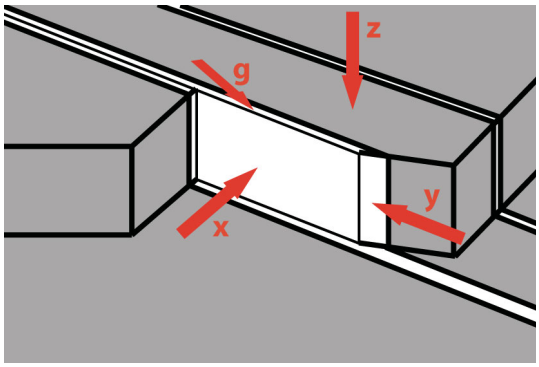

Fig. 16: Scheme illustrating the different predefined drilling orientations.

The orientations X, Y and Z are arranged like a Cartesian coordinate system relatively to the bedding in which Z is perpendicular to the bedding surface, Y is parallel to the striking of vein set 1 (cp. chapter 3.3.1) and X is perpendicular to the same striking. The g-orientation is supposed to be parallel to the expected linear, which defines the fibres of vein set 1.

2.1.7 Environmental sensibility

The aim is to take as few plugs as possible as core drilling has an irreversible impact on the environment and in addition to this, the location of the swimming pool pavement is a popular tourist spot. After taking plugs, holes are filled with concrete to minimize damage. Removal of all equipment, litter and all marks of the grid is self-evident in order to re-establish the former constitution of the spot.

2.2 Office-based work

2.2.1 Panorama generation

2.2.1.1 Processing raw data

The aim of processing the data is to optimize the picture quality. The processing focuses on the veins, as they are the point of interest. The raw data is existent in nef-format (Nikon-raw-codec) format. For further work with the pictures a batch conversion to jpeg format is necessary using Adobe Photoshop CS3 (Adobe 2007). The following processing properties are used for optimizing the pictures: white balance and exposure are levelled automatically; red / cyan fringe +18; sharpening amount +63 (with radius 1.3 and detail 25). The obtained processed pictures are grouped to the corresponding series:

- Series 1: DSC_0001 – DSC_0214
- Series 2: DSC_0215 – DSC_0272
- Series 3: DSC_0273 – DSC_0295
- Series 4: DSC_0297 – DSC_0380
- Series 5: DSC_0381 – DSC_0401

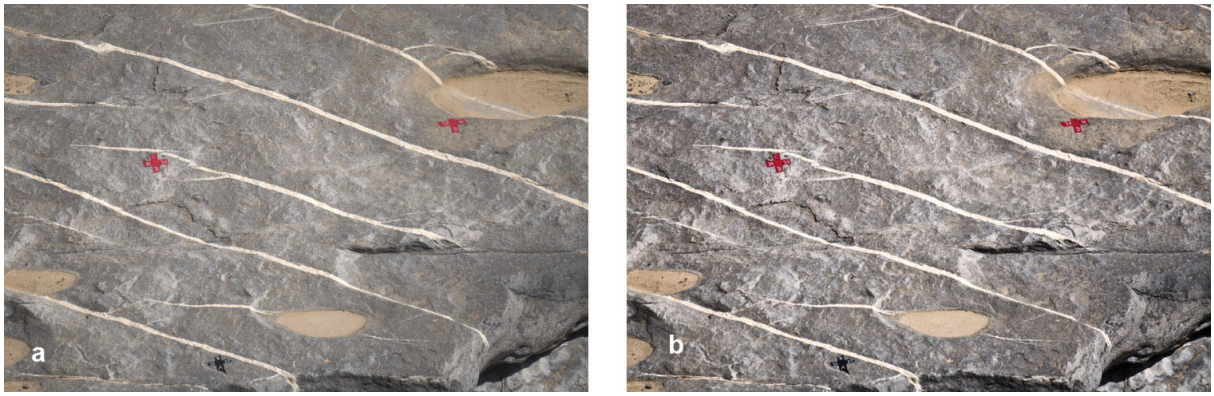

Fig. 17: The same picture a) prior to processing b) post processing.

2.2.1.2 Photomerge

The essential and critical part of the work is the photo merge. The program, which is used for the stitching is Kolor Autopano Giga 2.7 (Kolor); a software that creates panoramas, gigapixel images, etc. The program is able to handle large amounts of pictures; it merges them automatically but also provides an interface to influence the merging (AutopanoWiki 2009a). The software delivers a preview of the final image and calculates a value (RMS) describing the stitching-accuracy of the panorama. Each of the six fixed-spot series delivers an excellent RMS value testifying a good fitting of the images. In the case of an unsatisfactory RMS value at this stage of workflow it would be necessary to manually correct the stitching errors. By rearranging defined points that in reality lie on a straight line (i.e. the grid points), a tool of Autopano Giga performs a slight pre-rectifying.

The preview of the dipod series results in an unacceptable RMS quotient. Efforts for manual fixing are not successful. This series is therefore not used anymore for the following workflow. To obtain the panoramas, the other series are rendered to jpg-files using the smartblend (cp. Fig. 18) Blender and bicubic algorithm as interpolator (for further information about different rendering options and algorithms cp. AutopanoWiki 2008 & 2009b). Series 1 is rendered with 65% of the whole pixel amount; Series 4 with 75% (the adjustments for the other series are not mentioned because they are not short-listed for the final panorama. This is discussed in chapter 3.1.1). Test-renderings (images are attached on the DVD) with varying pixel amounts testify no information loss. Thus the file sizes are reduced, which increases the handling of the panoramas for further applications.

Both series are divided into two parts because the panorama dimensions clearly exceed the maximal accepted amount of pixels in a row or column by the jpg-format, i.e. 64000 pixels. Furthermore Adobe Photoshop CS3 only supports jpg-files with a maximum of 32000 pixels in a row or column. Other output formats, which could handle more pixels (e.g. TIFF), generate file sizes (>1 GB), which can not cope with the following work.

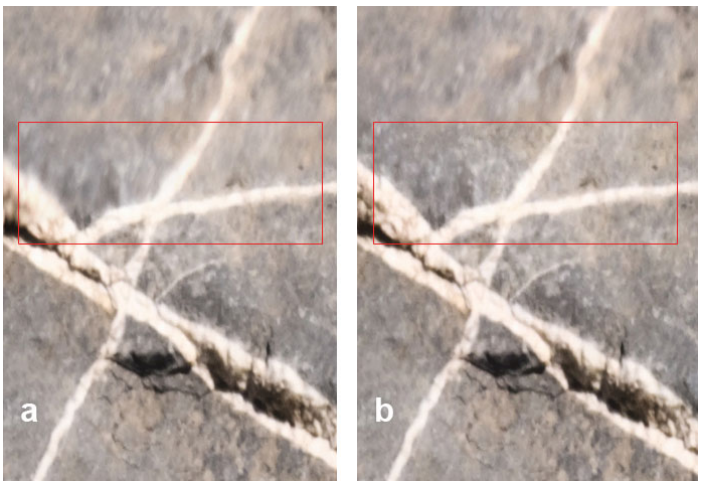

Fig. 18: Both pictures are rendered with Autopano Giga. For picture **a** the multiband Blender was used. The smartblend Blender was used for picture **b**. Within the red rectangle one can see a slight difference: the smartblend Blender delivers better results.

2.2.1.3 Rectification

As the viewing angle of the camera is not orthogonal onto the pavement, the panorama is optically distorted. This distortion needs to be adjusted for by the procedure of rectification. The idea is more or less to rotate the panorama (cp. Fig. 19) using the procedure described in the following:

This workflow is not carried out for each series, just for the selected series 1 and 4. The reasons for the selection are mentioned in chapter 3.1.1.3. The program used is ArcMap, which is part of the ESRI ArcGIS suite 9.3 (ESRI 2004). The rendered panoramas are loaded into the program as well as a grid of 2 m cell size (created with Microsoft Excel by entering coordinates). The tool 'Georeferencing' is used to distort the image with the result that the grid points marked on the pavement coincide with the grid points of the virtual grid. The algorithm used for the distortion is '*spline'.* The distorted picture is rendered to a new jpg file, conserving the adjustments and obtaining the rectified image. The result is comparable to a rotation of the panorama.

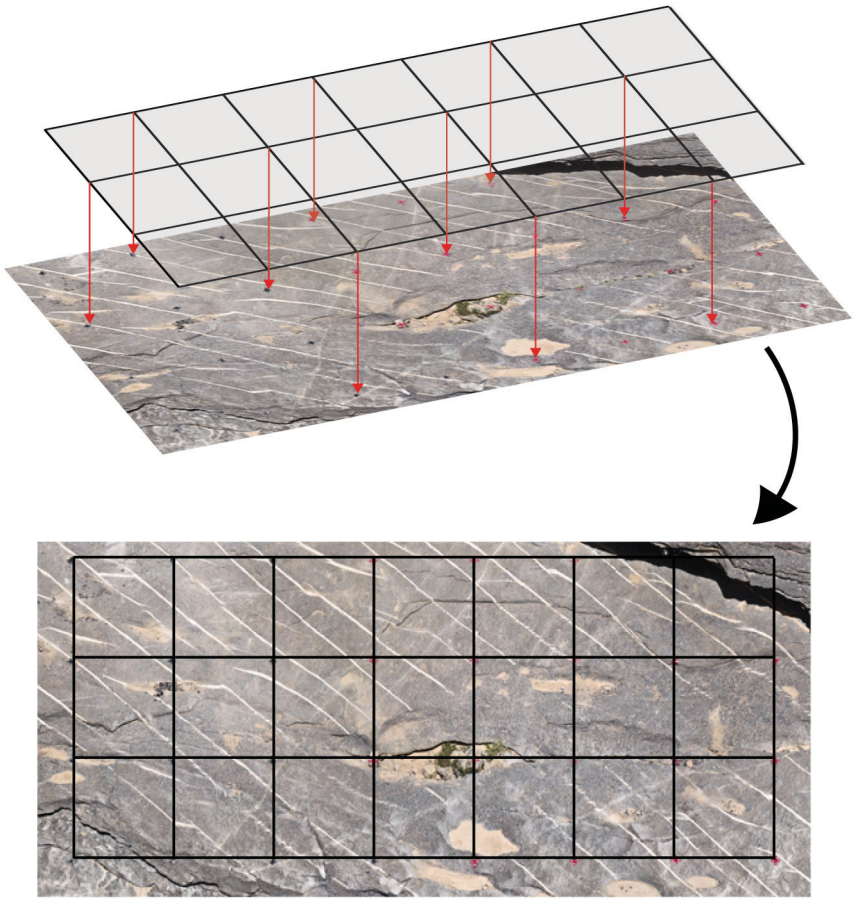

Fig. 19: Sketch showing the process of rectification via imaginary plane rotation.

Fig. 20: Picture **a** shows a section of the final panorama before a detail picture was integrated, whereas in picture **b** the detail picture is included.

2.2.2 Detail picture integration

The pictures of the detail work as well as the age relationship pictures are batch processed with the same parameters as the panorama pictures from raw format to jpeg format (cp. chapter 2.2.1.1). The pictures are integrated into the final panorama with the program Arc Map (cp. Fig. 20). Using the tool 'Georeferencing', the detail and age relationship pictures can be rearranged and distorted so that coinciding points have the same picture position. Manually coinciding points have therefore to be marked on each picture. For the distortion, the spline algorithm is used.

2.2.3 Sample preparation

As some of the plugs are broken or show cracks, which could lead to breakage during sample preparation, cyanoacrylate is used for the hardening of the cracks and the repair of already broken samples. As there are just a few samples available, it is of particular importance to find the most promising cut orientations (cut orientations are found in chapter 3.4). The samples are cut as defined and formatted to fit onto the glass slide. After the first polishing, the samples are glued onto the glass slides with epoxy resin. After hardening, the samples are cut once more. This should result in thin sample layers of approximately 1 mm on each glass slide. Finally the thin sections are polished again to a defined thickness of 30 µm.

3 Results and discussion

3.1 Panorama generation

3.1.1 The series

3.1.1.1 Resolution

The resolution of the panorama is of particular interest as it is strongly connected to the amount of data obtained by the panorama. This means concretely for example, the higher the resolution the smaller the observable structures.

Fig. 21: Both pictures have the same pixel dimensions and were shot from spot 1. Picture a is shot with a focal length of 200 mm, whereas picture b is shot with 400 mm. The resolution is clearly higher with 400 mm, although the effective resolution was digitally reduced during the rendering process of Autopano Giga.

3.1.1.1.(a) Focal length

The focal length directly affects the resolution. The aim of the different series with varying focal lengths was to test if outside influences – e.g. windy circumstances causing a camera shake – or objective defects affect the picture. It was considered that such influences could make the highest available resolution of the objective blurred. In this case the full range of the resolution can't be used and perhaps a smaller focal length would deliver the same results.

During the work it became clear that the series with the highest focal length (400mm) deliver the best results (cp. Fig. 21). They deliver the highest resolution even though the resolution was digitally reduced as explained in the chapter Material and Methods.

3.1.1.1.(b) Distance

The distance between the pavement and the imaging spot is the second parameter, which directly affects the resolution of the image: the smaller the distance the higher the resolution. Due to limited spot availability and the connection to viewing angle as discussed in the following, there is almost no chance of setting a favoured distance.

3.1.1.2 Viewing angle

The viewing angle is a further aspect, which has to be considered during the selection of the series. It affects the optical distortion of the image. This distortion has to be corrected by the process of rectification as explained in the chapter Material and Methods. The more correction that has to be done, the more errors can occur in the final image. As the panorama is intended to be a scientific dataset, it is favourable to use a viewing angle as close to orthogonality as possible.

In the case of the swimming pool pavement, the distance between the pavement and the imaging spot indirectly affects the viewing angle. As already described in the chapter Material and Methods, the viewing angle varies between both selected spots: spot 1 has a viewing angle of 43° and spot 2 has a viewing angle of 53°.

Fig. 22: Picture **a** and **b** illustrate the differences of image accuracy between the panoramas of series 1 and 4. Both pictures include the same integrated detail picture. The detail image of figure **a (series 1)** was distorted so much to fit into the panorama that the error is well visible: in reality, the veins are straight, as seen in the detail picture of figure **b (series 4)**.
Figures **c** and **d** show the same section of the outcrop and have the same scale (1:6,5). The figures should demonstrate that there is no significant information loss between the panoramas of series 1 and 4 (different spots, i.e. same focal length and different distance). Figure **c** is taken out of the panorama of series 1 (1,3 Gigapixel); figure **d** belongs to the panorama of series 4 (0,3 Gigapixel).

3.1.1.3 Selection of the series for the final panorama

It is self-evident and there is no doubt that the chosen series have to be the ones with the highest focal length, i.e. 400mm. It is strongly recommended for future projects to work with maximal focal length.

The decision as to the viewing angle is more difficult, it has to be made between a viewing angle closer to 90 degrees and the distance as described earlier. That means a decision between resolution and amount of optical distortion. For the final scientific panorama, the version with the viewing angle closer to orthogonality is chosen. The possibility of making more precise statistics, measurements etc. seems to be more important than the resolution.

Inter alia, following aspects were decisive:

The detail pictures used for the integration into panorama are all in map view (cp. previous chapters), so they have all an orthogonal viewing angle relative to the bedding. These pictures do not have visible distortions, at least if no major topography is present. During the process of integrating the detail pictures, it became evident that the panorama with the higher resolution had too many errors in the form of optical distortions. The detail pictures have to be distorted so significantly that the error is visually very easy to recognize. In comparison to this, the detail pictures integrated to the lower resolution version testify a relatively good result (cp. Fig. 22). This observation is consistent with another observation: in the panorama of series 1, the veins of set 1 (cp chapter 3.3.1) show a kind of 'waving', whereas in reality they are straight structures. This effect, caused by a not orthogonal viewing angle, is less present in series 4 compared to series 1 (cp. the attached panoramas on the DVD).

Apart from obtaining more precise results, visually there is no significant information loss in the lower resolution panorama detectable (cp. Fig. 22), i.e. smallest structures in the high resolution panorama are also recognizable in the lower resolution panorama even though they are not as detailed due to lower resolution. This is remarkable because the difference between the dimensions of both panoramas is quite large: series 4 has only 0,3 gigapixel whereas series 1 has 1,3 gigapixel, i.e. Series 4 has a dimension of roughly 23% of Series 4 but that doesn't cause a significant information loss.

In addition to the final scientific panorama, the high-resolution panorama will also be provided within this work. This enables the investigation of certain structures in a higher resolution if necessary, e.g. qualitative conclusions. Both panoramas combined deliver a good data set for further work.

3.1.2 Fixed imaging spot vs. dipod imaging

As already mentioned in the chapter Material and Methods, it was not possible to merge the pictures of the dipod series. The main problem with this method is the parallax effect due to motion of the optical centre combined with topography (cp. Arndt and Virgo 2010).

The effect can be understood by imagining two objects with differing distances to the observer. When the observer changes his position, i.e. changes the point of view, the two objects will change their position relative to each other. In reality the objects do not change position, it's just an optical effect, the parallax error (cp. Fig. 23).

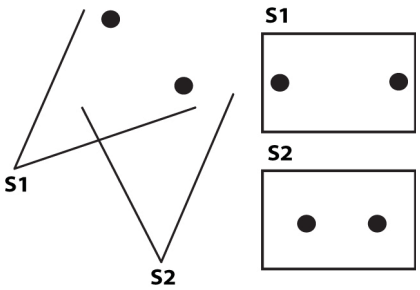

Fig. 23: Sketch illustrating the parallax error. From view S2, the points seem to have moved. In reality they didn't move but the viewing point changed.

The described effect makes it impossible for the panorama software to successfully stitch the pictures together, not even manual intervention generated a satisfying result. As it is not possible to generate a panorama it is not recommendable to use this technique for further projects. A second disadvantage is the lavishness of this technique compared to the fixed spot alternative. Eventually it is evident that imaging from a fixed spot is the correct choice.

3.1.3 Detail picture acquisition for integration into panorama

The acquisition of detail pictures is a useful addition to panorama generation in several ways: It delivers higher resolution images from points of interest; it gives the opportunity for a quality check for the rectification of the panorama (cp. chapter 3.1.1 and Fig. 22) and other thinkable applications.

For the acquisition one aspect has to be kept in mind: Pictures of spots with morphology such as edges of layers cannot be satisfactorily integrated if the viewing angle of the detail picture and the panorama do not coincide. Pictures with these circumstances should be avoided; the integration into the panorama leads to an unacceptable distortion (as seen in Fig. 22).

3.1.4 Proposals for future projects

In order to achieve an efficient and successful panorama generation, following aspects have to be kept in mind. As the development of this technique is still at its beginning, it is self evident that a panorama can not be successfully generated for every type of outcrop. The problem of topography is evident, even topography of smaller scale can cause problems, which became clear during detail picture integration as discussed in the previous chapter. Problems caused by topography in general are well demonstrated and discussed in the co-work of Thronberens (2010). In conclusion, a preferably flat outcrop with a homogeneous dip

of the surface is preferable and a factor for accuracy of the panorama. The smaller the difference between the real outcrop and the imaginary plane lain over the outcrop, the smaller the errors in the form of distortions caused by topography.
The second factor of major importance is the viewing angle. As discussed in chapter 3.1.1.2ff, even small differences clearly affect the accuracy of the panorama. Thus it appears that the imaging spot should provide a viewing angle as close as possible to orthogonality. The resolution is also important and it is essential to obtain the highest resolution as possible. However, it should be considered secondarily referred to the viewing angle, i.e. if there is no grave information loss because of smaller resolution, the spot with the angle closer to orthogonality should be chosen.
An angle closer to orthogonality could also make it possible to generate an image of an outcrop with slight topography as was seen during the process of the detail image integration: the small scaled topography of the swimming pool pavement only led to a few errors; the image accuracy is satisfactory (cp. Fig. 20b and detail images integrated into the panorama, attached on the DVD). On the other hand, an almost entirely flat outcrop can probably be imaged with a smaller viewing angle of acceptable accuracy. This can be seen in the co-work of Raith (2010).
All in all, it is not possible to define an explicit working advice. The different factors interact; a final decision can only be made by balancing the different factors for each outcrop situation.

As viewing angle is the critical factor, improvement of the technique could be reached by delocalizing the fixed imaging spot away from the ground surface. An approach to solve this could be aerial imaging; the critical requirement would be the fixed spot, i.e. no moving of the camera during image acquisition, thus a stationary camera setup.

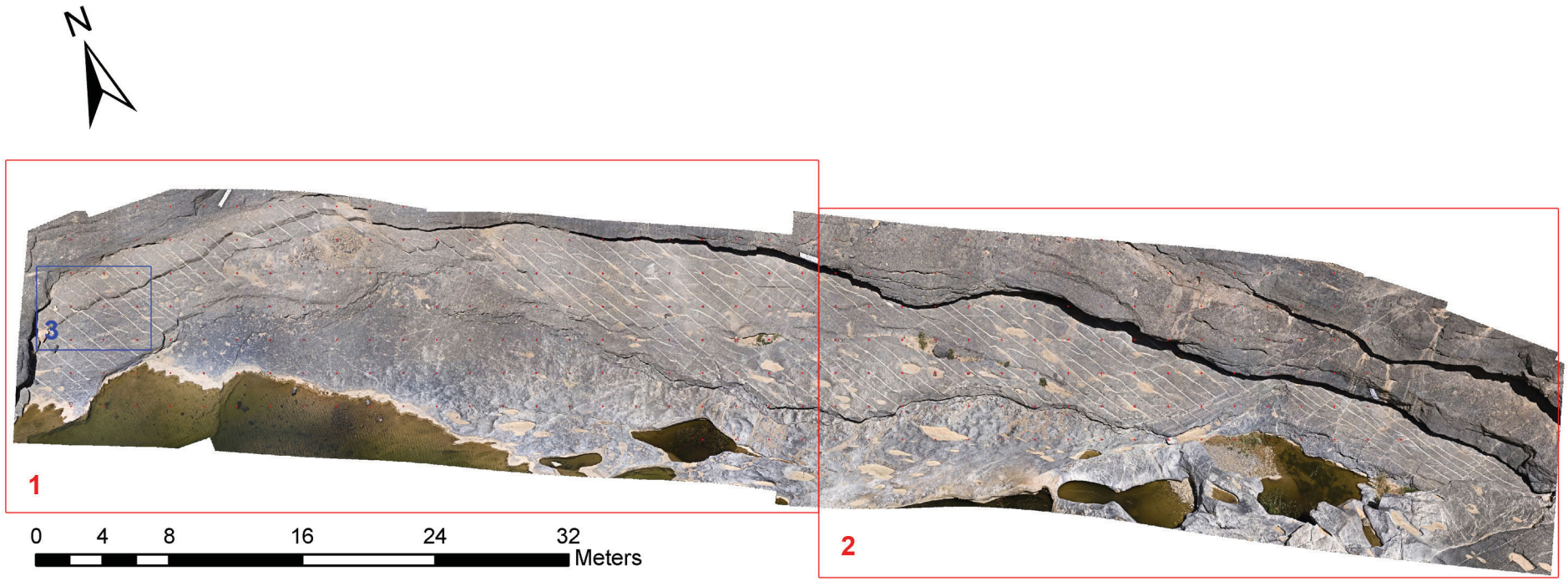

Fig. 24: Overview image of the final panorama of series 4. The red frames mark the zoom series of the pavement on the following pages (Fig. 25 to Fig. 32). The blue frame marks the area of the map of the plug positions (Fig. 38). The scale of the image is 1:380.

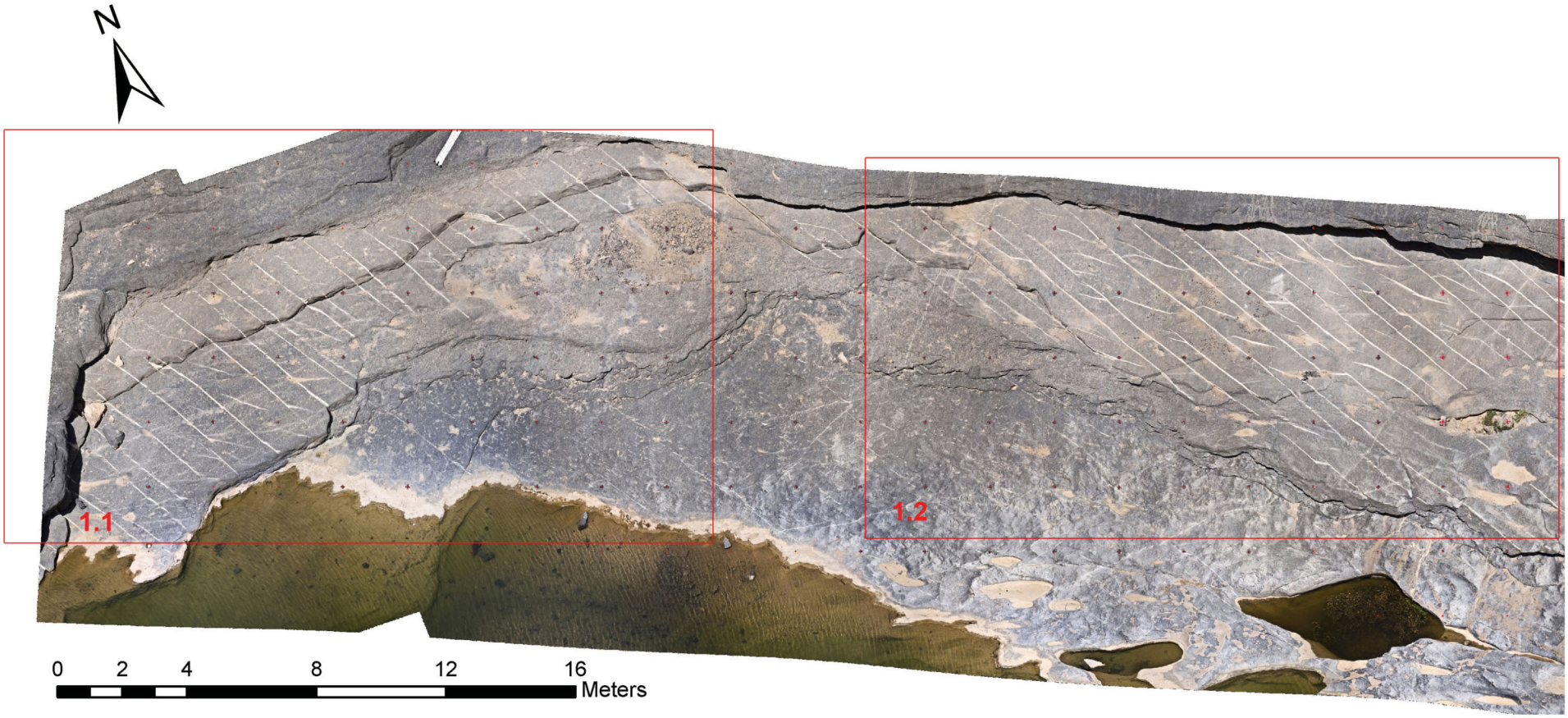

Fig. 25: The figure is part of zoom series 1 (Area 1 in Fig. 24). The scale of the image is 1:190.

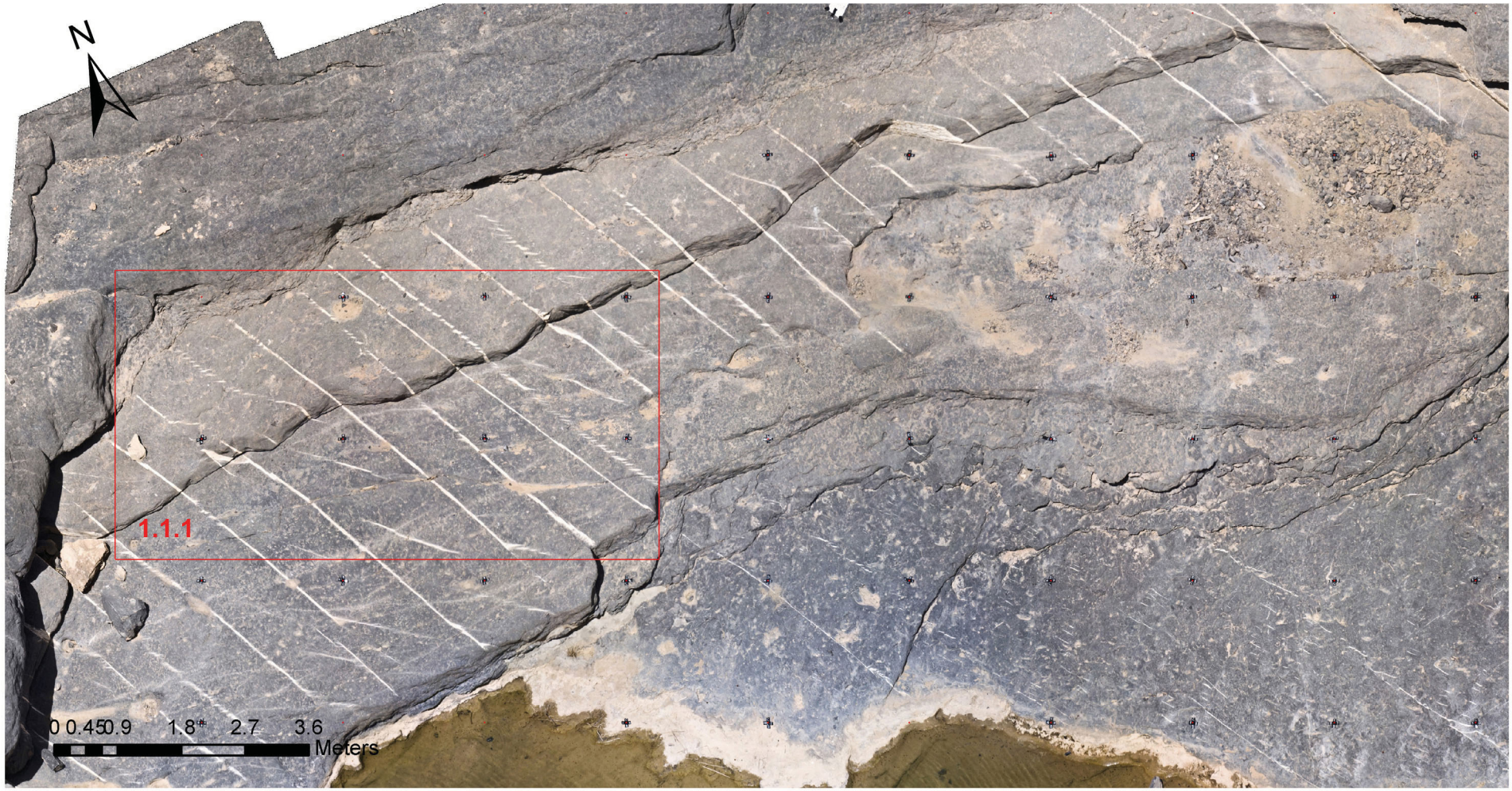

Fig. 26: The figure is part of zoom series 1 (Area 1.1 in Fig. 25). The scale of the image is 1:85.

Fig. 27: The figure is part of zoom series 1 (Area 1.1.1 in Fig. 26). The scale of the image is 1:30.

Fig. 28: The figure is part of zoom series 1 (Area 1.2 in Fig. 25). The scale of the image is 1:85.

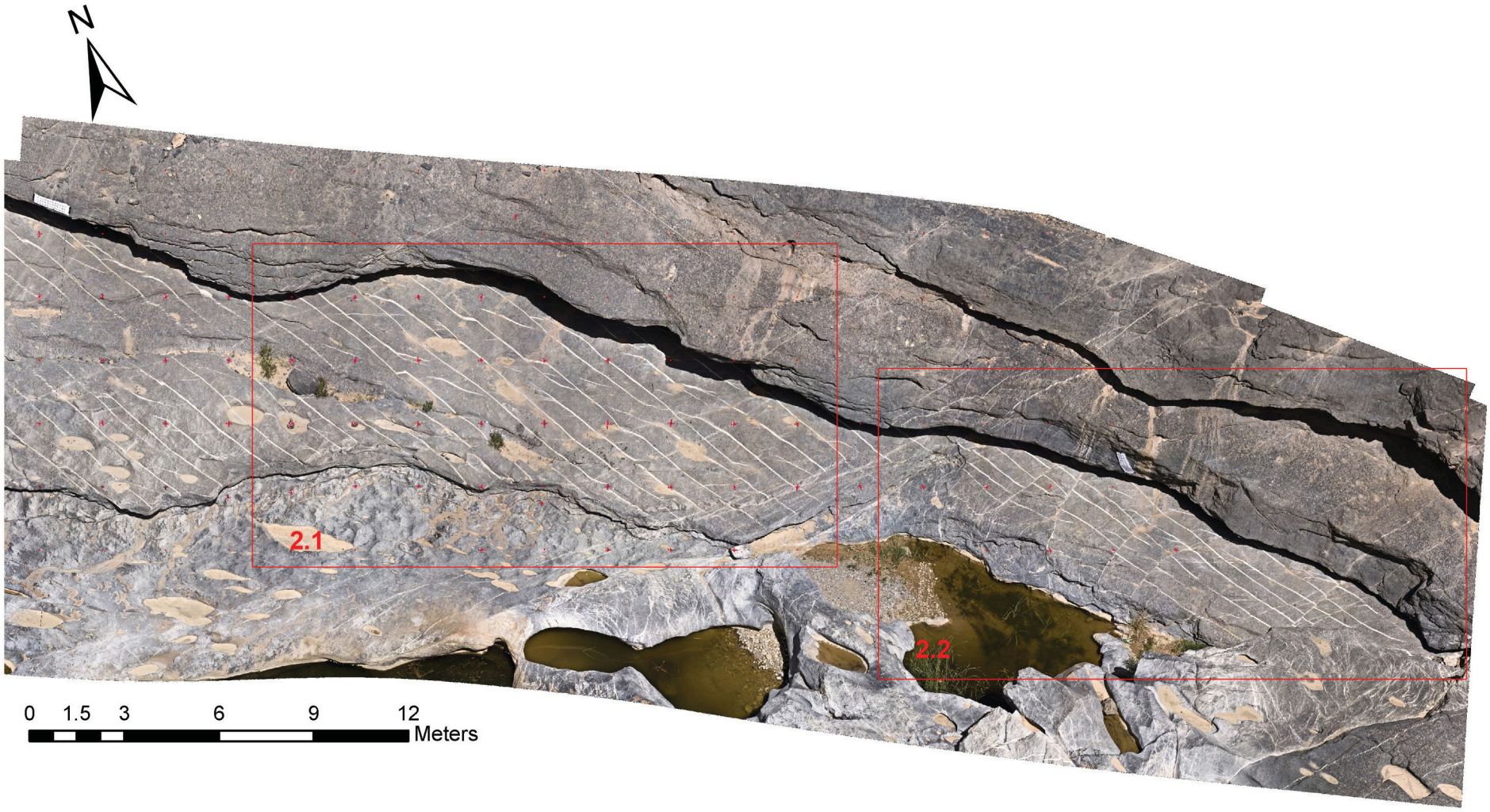

Fig. 29: The figure is part of zoom series 2 (Area 2 in Fig. 24). The scale of the image is 1:190.

Fig. 30: The figure is part of zoom series 2 (Area 2.1 in Fig. 29). The scale of the image is 1:75.

Fig. 31: The figure is part of zoom series 2 (Area 2.2 in Fig. 29). The scale of the image is 1:75.

Fig. 32: The figure is part of zoom series 2 (Area 2.2.1 in Fig. 31). The scale of the image is 1:30.

3.2 The final panorama data set

The final dataset consists of the 0,3 gigapixel panorama (Fig. 24), created of the pictures of series 4; containing 84 images shot from spot 2 with a focal length of 400mm. The dimension of the panorama is roughly 35000 x 8986 pixels, which images a 90 m x 12 m outcrop. The scale is roughly 1:9. Detail pictures, microstructural images and plug positions are integrated into the panorama. It has to be kept in mind that the grid is not N-S oriented, but is rotated 20° clockwise. As previously mentioned, the panorama created of series 1 is also provided, thus one can compare both panoramas and it allows for the investigation of certain structures in a slightly higher resolution where necessary. The 1,3 gigapixel panorama consists of 213 images shot from spot 1 with a focal length of 400mm. The dimension of the panorama is 77115 x 19006 pixels. The scale is roughly 1:5.

3.3 The vein network

The data obtained by the detail work on the pavement can be grouped into two datasets: One dataset includes dip direction and dip of each measured vein, the other dataset just includes the striking of the measured veins projected onto a horizontal plane. A 3D measurement wasn't possible for the second type of dataset. For statistics and stereo plotting just the first dataset is used, nonetheless the results of the second dataset are consistent with the results of the first dataset. Generally two sets of vein generations can be clearly defined, a third one is yet to be discussed. Apart from these main vein sets, several structures related to the principal vein sets appear repeatedly in the outcrop.

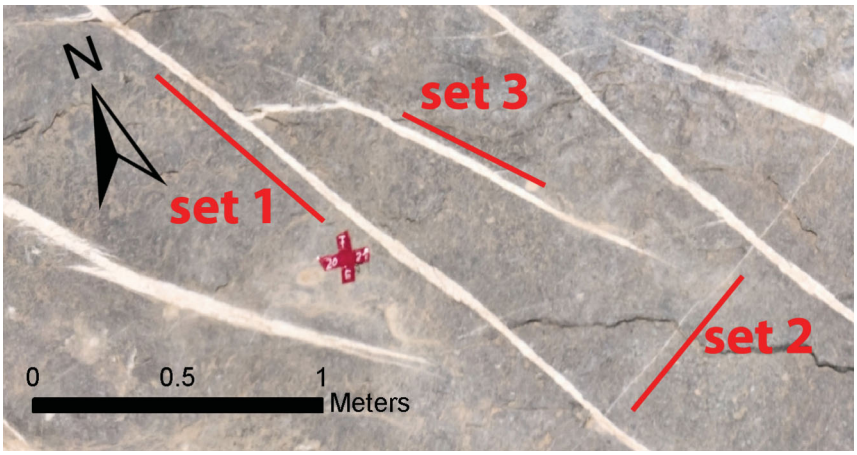

Fig. 33: Section of the panorama / outcrop showing the three sets of veins. Set 2 has only a small aperture compared to the other sets.

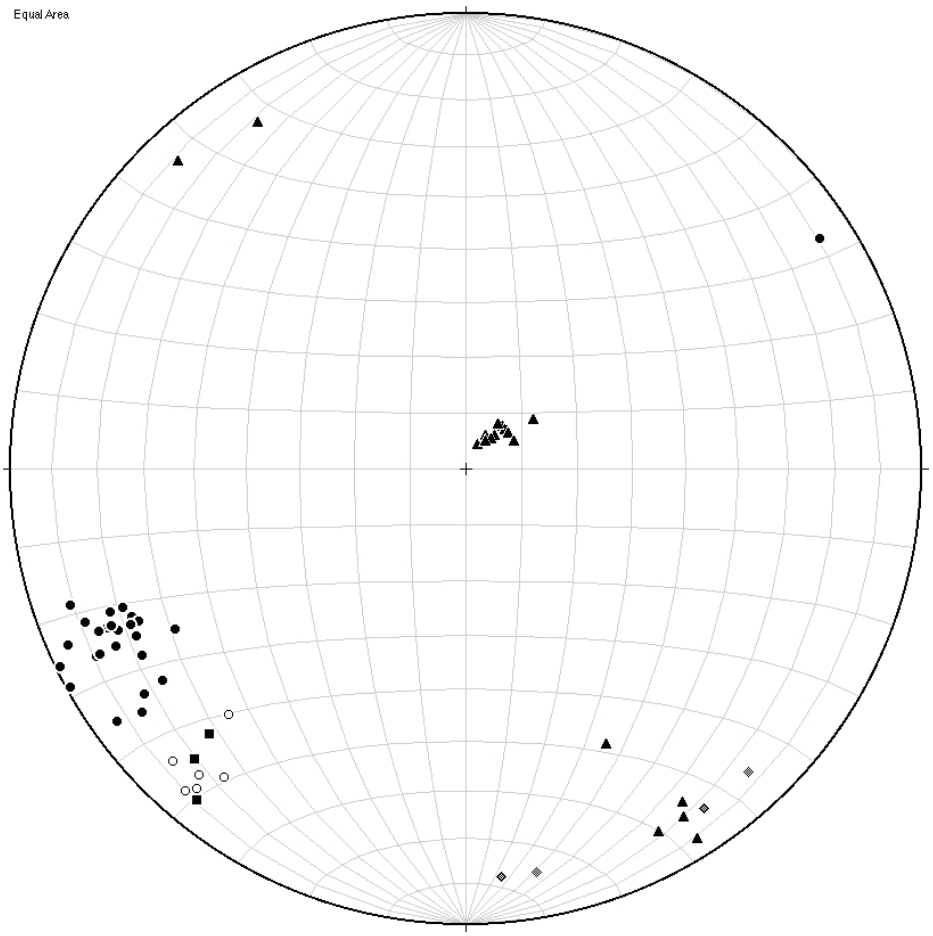

Fig. 34: Stereoplot of the measured veins. Filled circles mark set 1; filled triangles mark set 2; filled squares mark set 3; hollow circles mark wings and splays of set 1; diamonds mark fault related veins; cluster of filled triangles in the centre represents the bedding.

3.3.1 Set 1

This set of veins is easily identifiable already by regarding the panorama of the outcrop. The averaged dip direction and dip of the vein set is 063°/75°. The cluster of plane normals is well visible in the stereo plot (cp. Fig. 34). Measurements of the aperture deliver an averaged value of 3 cm but with a standard deviation of 0,7 cm; therefore this value should be considered more as a dimension of the aperture. Set 1 contains blocky as well as fibrous veins (just macroscopic investigation). Some veins can be investigated in 3D (cp Fig. 35), some of the veins were exposed in a way, so one can see and measure their fibre directions (cp. Fig. 35), delivering an averaged fibre linear of 160°/23°. This value is not representative because it is based on an insufficient amount of measured values to be representative. However it may give a rough indication as to the real fibre direction. At several spots the fibre direction was measured in 2D, i.e. the observed fibre direction was measured as a striking value projected onto a horizontal plane. These observations deliver a striking value of 170°.
Tabular veins as well as en echelon sets are observable in set 1. The en echelon sets and tabular veins can't be regarded separately: At some special spots one can see that tabular

veins somehow fan out to en echelon spots (cp. Fig. 36). The observed en echelon sets are all of a sinistral shear sense and appear in sigmoidal as well as in lenticular shape. The averaged orientation of the en echelon set is a striking (projected onto a horizontal plane) of 116°. Features which are observed quite commonly are wings and splays of set 1, with an averaged dip direction and dip of 042°/77°. A connection between two veins of set 1 called ‘step over’ is observable at several spots.

Set 1 is consistently present in layer I and II with apparently relatively constant distances between the veins (cp. Panorama). In layer III set 1 is not present at least without the same characteristics as for example frequency or dimension of aperture. However, Layer III wasn’t part of the detail investigation due to the limited time-frame. Conclusions about layer III therefore are speculative.

Fig. 35: The figure shows a vein of set 1 exposed in 3D. Lineation seen on the vein plane allows for a measurement of the fibre direction.

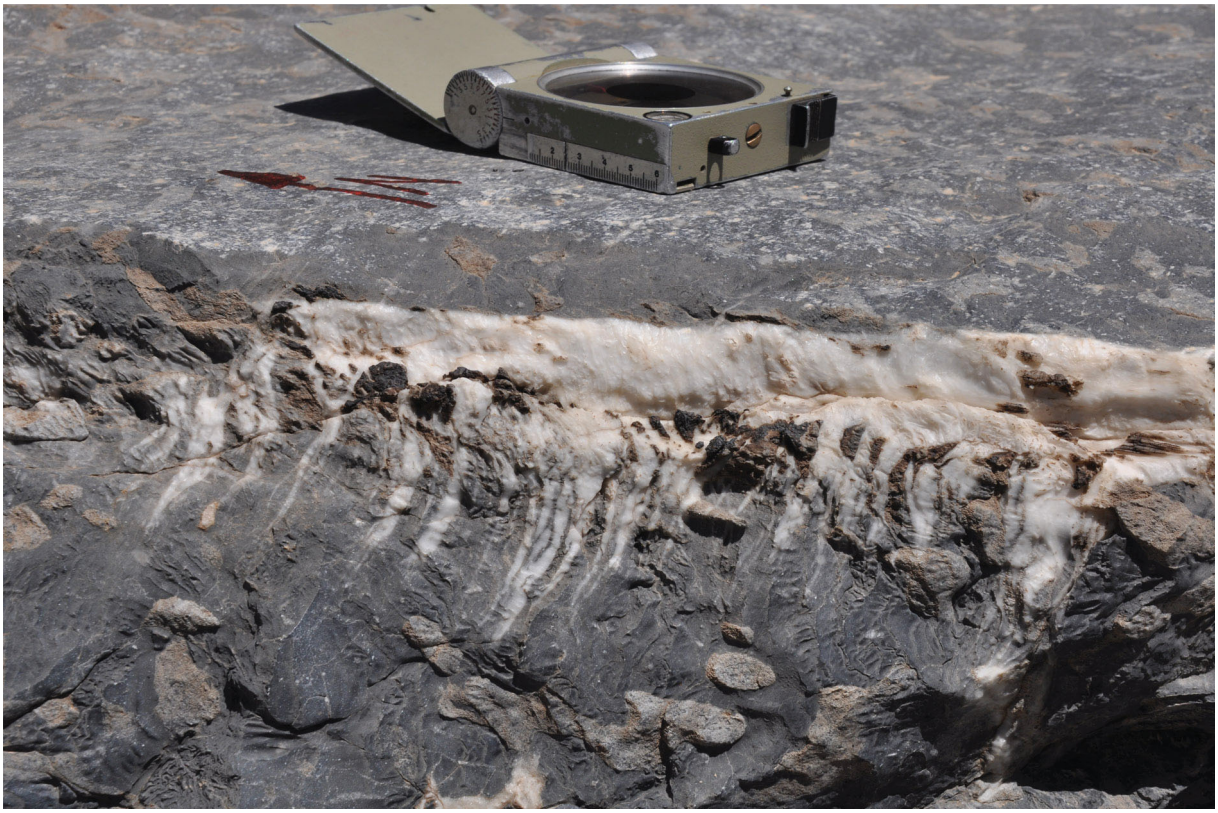

Fig. 36: Fan out of tabular veins to en echelons.

3.3.2 Set 2

Veins of set 2 are clearly not as frequent as veins of set 1 and have a much smaller aperture of an approximate dimension less than 0,5 cm. The averaged dip direction and dip of this set is 329°/75°, based on too few values to be representative. In the stereo plot (Fig. 34) a small cluster of set 2 is visible. Two values on the opposite site of the stereo plot can be classed as belonging to the same cluster as the dip is close to 90 degrees and measurement inaccuracies can cause the 180° difference of dip direction. Set 2 is clearly present in Layers I and II. As true for the previous set, information relating to Layer III is missing due to the limited time-frame.

3.3.3 Set 3

The averaged dip direction and dip is 040°/78°. As also seen in the stereo plot, there is a noticeable analogy between the values of the splays and wings of set 1. Their relationship to set 1 could be a point of discussion and maybe worth further investigations. The dimension of aperture is the same as that of set 1.

3.3.4 Fault related veins

In the western part of the outcrop, veins are found of an approximately similar orientation as that of set 2, visible in the stereoplot (Fig. 34). Probably they are related to a fault, which crosses the outcrop in this area. Age relationships with offset, discussed in the following, coincide with this interpretation. The crossing fault and the geology on a larger scale are discussed in the work of Laurich (2010).

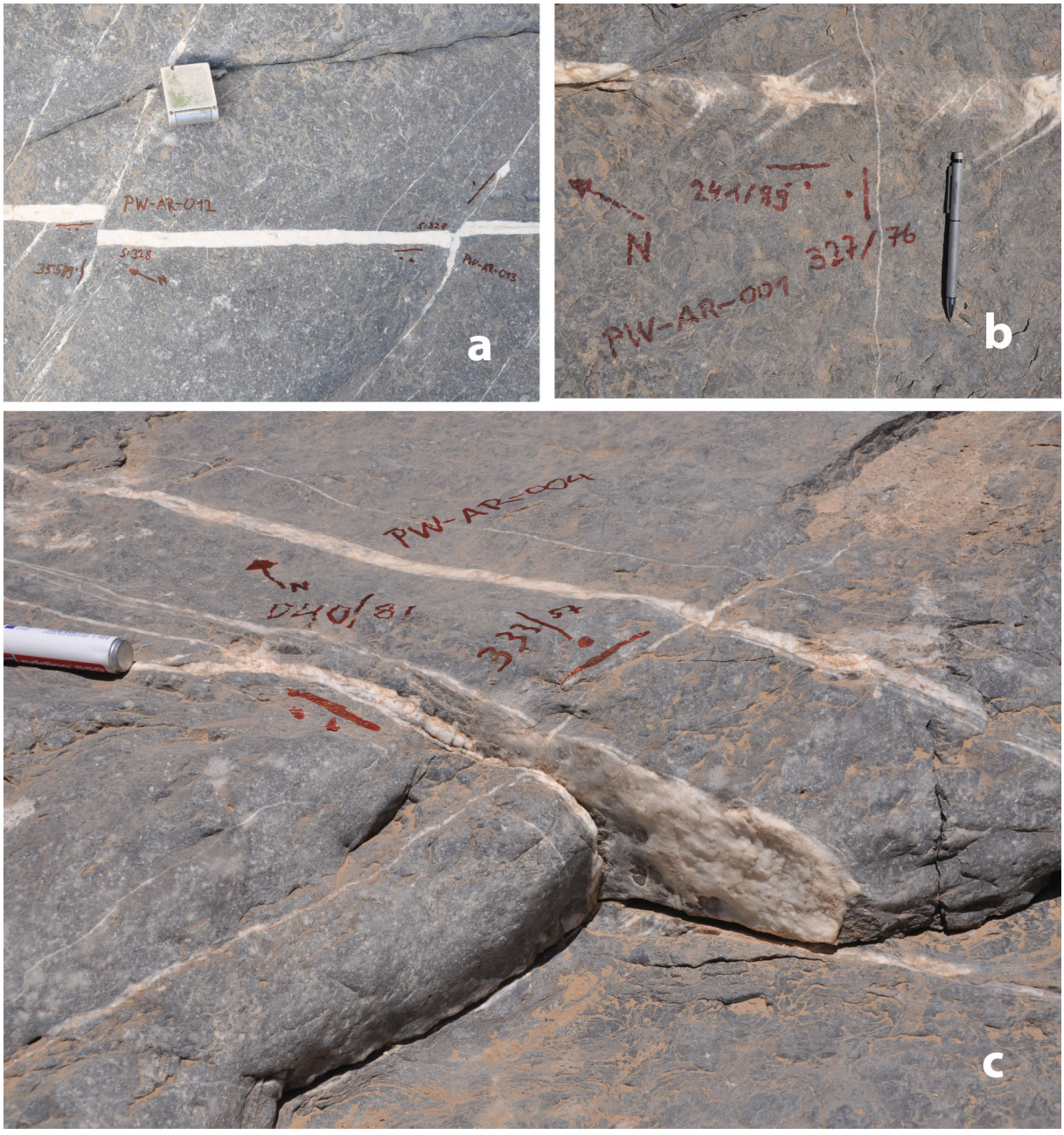

Fig. 37: Age relationship images. Figure **a** represents age relationship 2: vein of set 1 is crossed by fault related veins. One can see sinistral and dextral offset. Figure **b** represents age relationship 1: a vein of set 2 crosses en echelons of set 1. In figure **c** a 3D age relationship of set 1 and 2 is exposed.

3.3.5 Age relationships

The age relationship investigation delivers two principal results:

3.3.5.1 Age relationships 1

The age relationships visible in Fig. 37 clearly show that set 1 is crossed by set 2, therefore the event resulting in the veins of set 2 is younger than the event from which the veins of set 1 evolved. This age relationship is consistent for tabular veins and en echelon sets of set 1.

3.3.5.2 Age relationships 2

These age relationships are concentrated in the eastern area of the outcrop, previously mentioned as the area with a crossing fault. Set 1 (probably slightly rotated because of the fault nearby) is crossed by the previously mentioned fault related veins. Predominantly dextral offset can be observed at set 1. Sinistral offset can be found as well (cp. Fig. 37), maybe belonging to a conjugated set.

3.4 Microstructure

In each thin section two principal phases are present: calcite and quartz. The main criteria for the differentiation of both phases are polarization colours and twinning of the calcite crystals. Calcite often shows polarization colours of higher orders, whereas quartz shows colours of the first order, typically black to grey (except in thin sections with a thickness variation). The plug positions can be found in Fig. 38, overview images are attached in the appendix (full resolution images on the DVD).

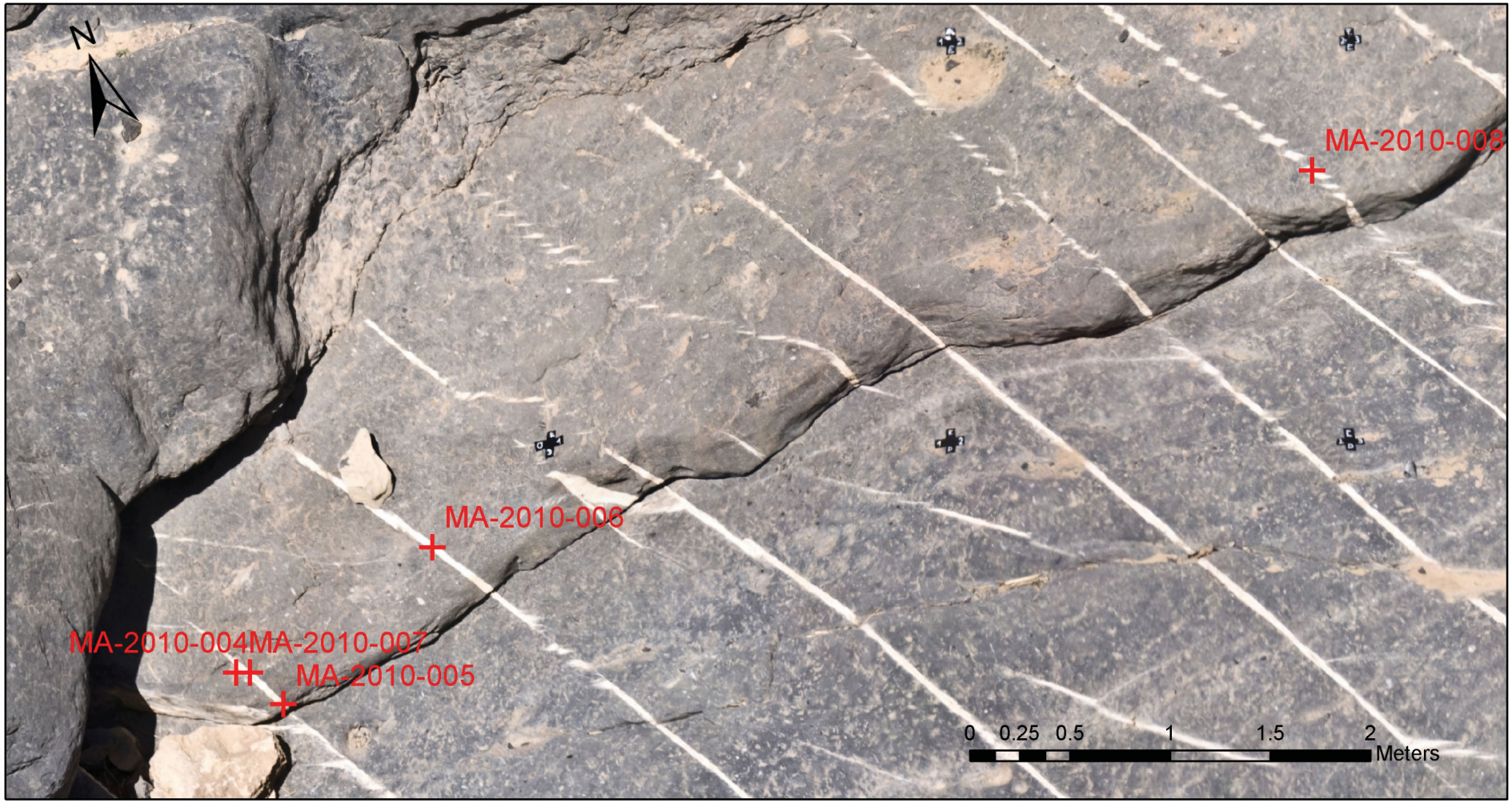

Fig. 38: Map of plug positions. Area 3 in Fig. 24 represents the section of this map. The scale is 1:30

3.4.1 MA-2010-004

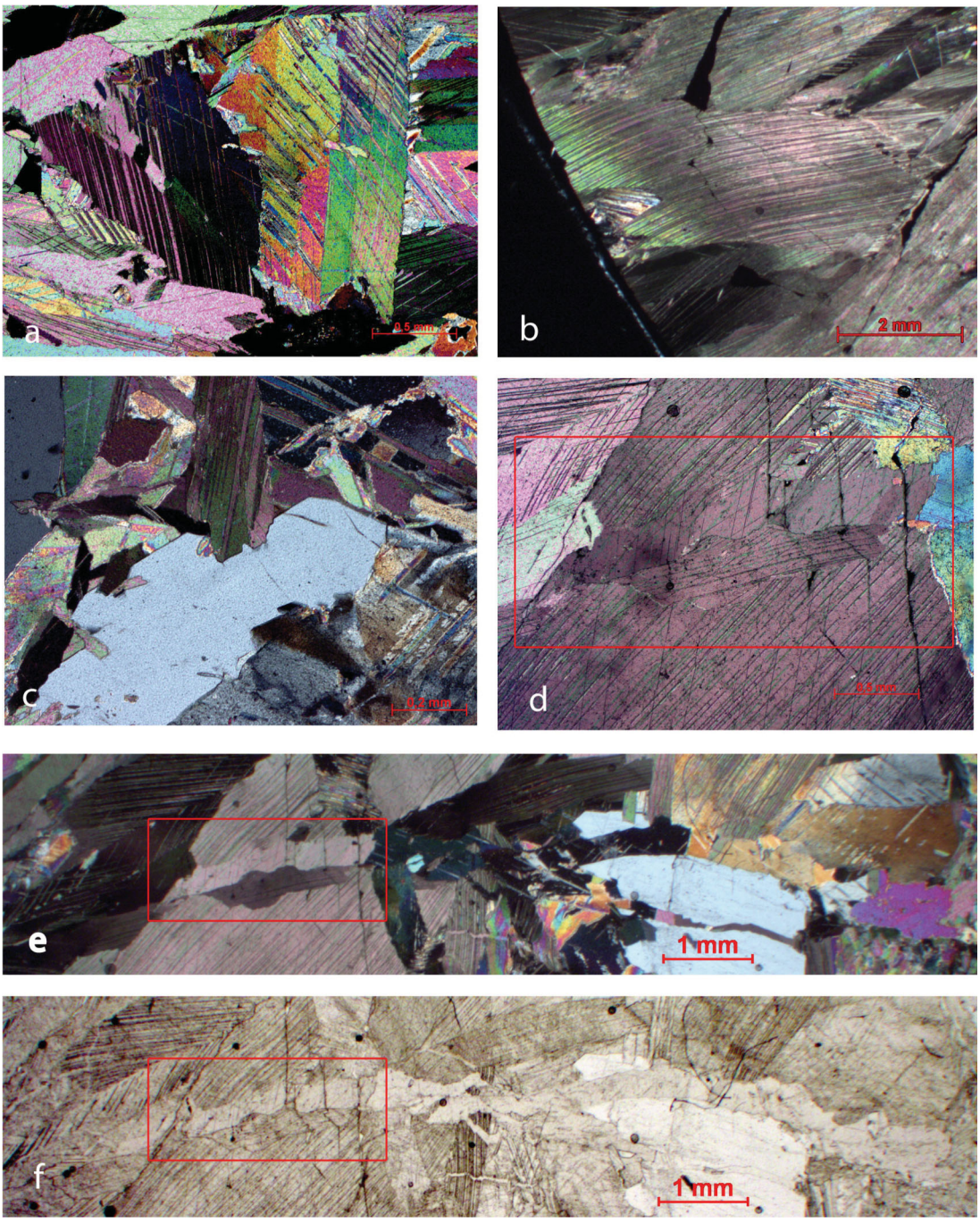

Fig. 39: Polarized images of thin section MA-2010-004. **a)** Straight twinning of calcite. **b)** Curved twinning of calcite. **c)** Hypidiomorphic quartz grain. **d)** Part of the microcrack shown in figure e & f (highlighted with red frame). The evidence for epitaxial grain growth is well visible: the microcrack can just be identified by different twinning characteristics compared to the surrounding material **e)** & **f)** Microcrack filled with epitaxial grown calcite grains under polarized light and without crossed niccols.

The plug for this thin section was drilled in z-orientation (cp. chapter 2.1.6.2) with a drilling linear of 049°/81°. The cut for the thin section is perpendicular to the drilling linear and therefore has a plane orientation of 229°/29°, which is more or less parallel to bedding and perpendicular to the vein defined by the plane 062°/88°.

Both main phases calcite and quartz are present in the thin section with a roughly 90/10 composition. Calcite often shows idiomorphic grain shapes. Twinning is well observable, showing both a straight and a curved shape as visible in Fig. 39a&b. There are just a few quartz aggregates present in the thin section. The grains show undulose extinction; subgrains are detectable. Compared to the other thin sections discussed later, the quartz grains have just relatively few fluid inclusions. Clearly idiomorphic grains were not found, most of the grains / aggregates appear to be xenomorph. Some grains were found which appear to be hypidiomorphic as shown in Fig. 39c. The grain seen in this picture shows both, crystal planes which belong to the quartz crystal lattice and planes, which belong to another crystal lattice, probably to the one of calcite. Fragments of the calcite phase within some quartz grains are present; this may refer to contemporaneous grain growth. Host rock is well visible without crossed niccols, but just the host rock of one site of the vein. The boundary between host rock and vein (in the following abbreviated with 'HVB' for host rock - vein - boundary) is diffuse, therefore not easily definable. The host rock composition is micritic and sparitic including primary structures like fossils. Microcracks, which are parallel oriented to the HVB, are well visible without crossed niccols and quite frequent. Host rock fragments seem to be included into vein material, which indicates the process of crack seal.

Another set of microcracks shows an approximate average direction perpendicular to the HVB. This set of microcracks crosses the HVB and is also present in the vein area, as for example the relatively big microcrack seen in Fig. 39f. This crack is filled with epitaxial grown calcite grains; under crossed niccols it can just be identified by different twinning characteristics compared to the surrounding material (cp. Fig. 39d&e). The size of this explicit microcrack is not representative for this set of microcracks, especially in the host rock area, where they appear with smaller sizes.

A homogeneous area in the form of a thin band next to the host rock area can be defined by the common grain characteristic of shape preferred orientation perpendicular to the HBV. Compared to the remaining thin section, this homogeneous area includes relatively small grains. In the centre of the thin section the average grain size is the largest. With exception of the previously defined area, no other homogeneous area can be defined by the same characteristics. The ordering of the crystals seems to be of a more chaotic nature.

3.4.2 MA-2010-005

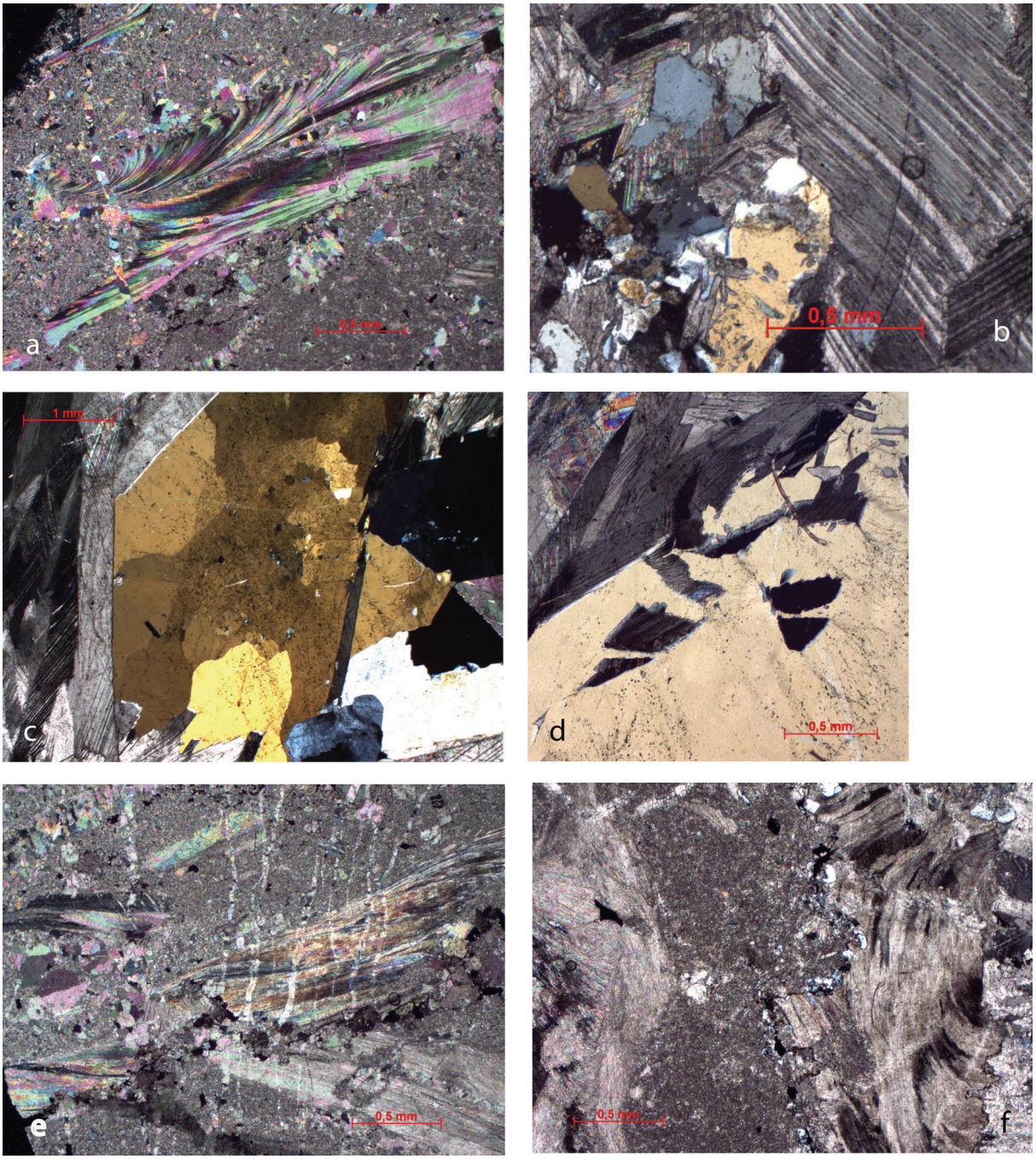

Fig. 40: Polarized images of thin section MA-2010-005. **a)** Micritic host rock area including primary structures. **b)** Slightly curved twinning of calcite grains and a hypidiomorphic quartz grain. **c)** Subgrains in xenomorphic quartz grain. **d)** Calcite fragments within quartz grain. **e)** Several microcracks crossing a primary structure in host rock area. **f)** Stylolithe in host rock area.

The plug was drilled in y-Orientation (cp. Fig. 16), with a measured drilling linear of 338°/07°. The cut orientation of the thin section is perpendicular to the drilling linear and therefore has a cutting plane orientation of 158°/83°. The sample was broken during the drilling process. The main phases calcite and quartz are present with a roughly 80/20 composition. Generally twinning is well seen in the calcite phase. Straight and curved (cp. Fig. 40b) shaped twinning are both observable. The calcite grains predominantly seem to be idiomorphic. Undulose extinction is observed in the quartz phase as well as subgrains (Fig. 40c). Fluid inclusions are present in most grains. The quartz grains do not show a clear idiomorphic grain shape but at least hypidiomorphic grains are detectable as shown in Fig. 40b.

The HBV is diffuse but observable without crossed niccols. The composition of the host rock is predominantly micritic with primary structures such as the fossils shown in Fig. 40a. Closer to the HBV the composition becomes at least partly sparitic. Microcracks are well visible in the host rock area, for example a microcrack, which crosses a primary structure (cp. Fig. 40a&e). Stylolithes are present in the area of the HBV (cp. Fig. 40f). Small quartz grains are located at the stylolithes; they didn't dissolve.

In comparison to other grains, three relatively big quartz grains are present in the thin section. These grains differ slightly, not only because of their grain size: At least one of these quartz grains appears to be xenomorph, the grain's shape shows calcite lattice planes of the surrounding calcite grains (cp. Fig. 40c). In general the grain shape of these larger quartz grains is blockier, at least when compared to the surrounding grains. Calcite grains are found within a quartz grain (cp. Fig. 40d)

A homogeneous area can be defined close to the HBV, drawn onto the overview image. The criteria for homogeneity is a supposed shape preferred orientation perpendicular to the HBV. Compared to the other parts of the thin section (with exception of the host rock), grain size is small. Other homogeneous areas can't be defined by the same criteria, although a trend to a shape preferred orientation - parallel to boundary between host rock and vein – in the centre of the thin section is recognizable.

3.4.3 MA-2010-006

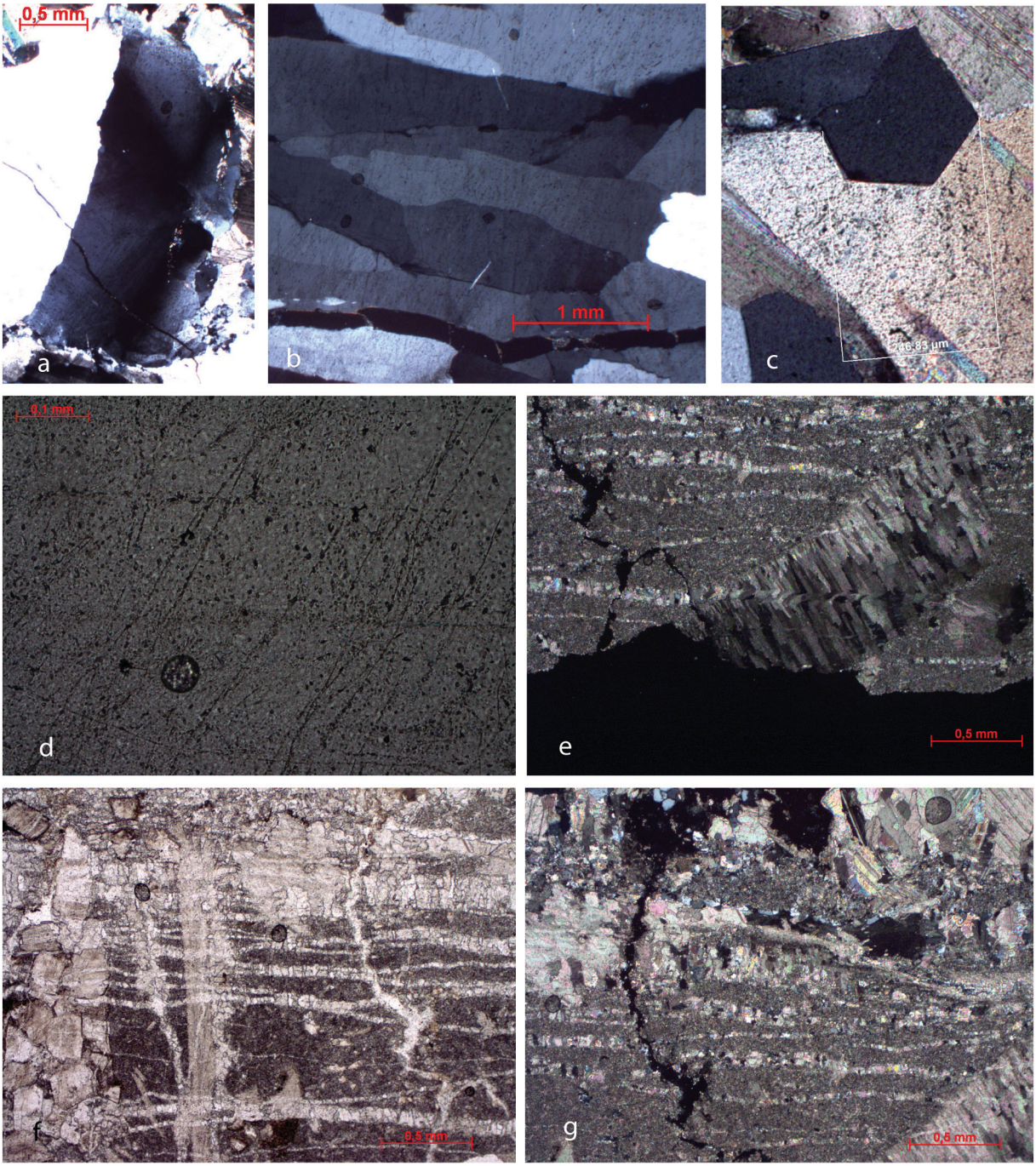

Fig. 41: Polarized images of thin section MA-2010-006. **a)** Undulose extinction of quartz grain. **b)** Subgrains of quartz. **c)** Idiomorphic quartz grain. **d)** Fluid inclusions in quartz grain in the form of bands in specific directions. **e)** Microcracks crossing primary structures. The cracks appear to be epitaxial grown. **f) & g)** Microcracks in host rock area filled predominantly with calcite, but also with quartz. Polarized image and image without crossed niccols.

The plug of this thin section was drilled in supposed g-orientation. The drilling linear is defined by 195°/55°. The cut of the prepared thin section is calculated to be horizontal. Therefore it is roughly parallel to bedding. The plug was taken in sector D0 and was broken during the drilling process. Both main phases are observable: Calcite and quartz with an approximate 70/30 composition. The thin section varies in thickness, noticeable because of different polarization colours in the calcite phase (cp. A. 4). Generally twinning of the calcite phase is well observable, both straight and curved. Calcite seems to be predominantly idiomorphic.

The quartz phase of the thin section shows undulose extinction as visible in Fig. 41a as well as subgrains as shown in Fig. 41b. Further features, which can be observed, are fluid inclusions in the quartz phase. They can be found randomly as well as in the form of bands in specific directions (cp. Fig. 41d). At some locations, idiomorphic quartz crystals can be identified, e.g. in Fig. 41c. Other sections show hypidiomorphic quartz grains; these grains show both: crystal planes, which belong to the quartz lattice as well as planes that can be related to the neighbouring calcite lattice.

As in previously discussed thin sections, the HBV is diffuse but observable without crossed niccols. The host rock is predominantly micritic with primary structures such as fossils. Microcracks are visible in the host rock, filled predominantly with calcite but also with quartz Fig. 41f&g. By the observation of primary structures, microcracks are visible, these cross these structures and appear to be epitaxial at least at some distinct spots (Fig. 41e).

With exception of the host rock, two homogeneous areas can be defined. The first homogeneous area is defined by shape preferred orientation of the crystals perpendicular to the HBV followed by a band of grains with a more blocky grain shape. The grains in this area are relatively small compared to grains of other homogeneous areas except for those from the host rock areas. It is noticeable that the quartz grains in the domain with the shape preferred orientation have less fluid inclusions than the domain with the blocky grain shape and other homogeneous areas. The second homogeneous area seems to be the most characteristic part of this thin section; it directly catches the observer’s eyes. Both principal phases, calcite and quartz, appear well separated in the form of two main bands, crossing the thin section from one side to the other. The grain size is larger than in other parts of the thin section.

A shape preferred orientation of the grains of both phases is clearly observable and is orientated approximately parallel to the boundary between host rock and vein. Fluid inclusions of quartz in this area are usually arranged in bands, as shown in Fig. 41d. The rest of the thin section does not show a consistent common feature, which could define another homogeneous area. Parts of it seem to be chaotic.

3.4.4 MA-2010-007

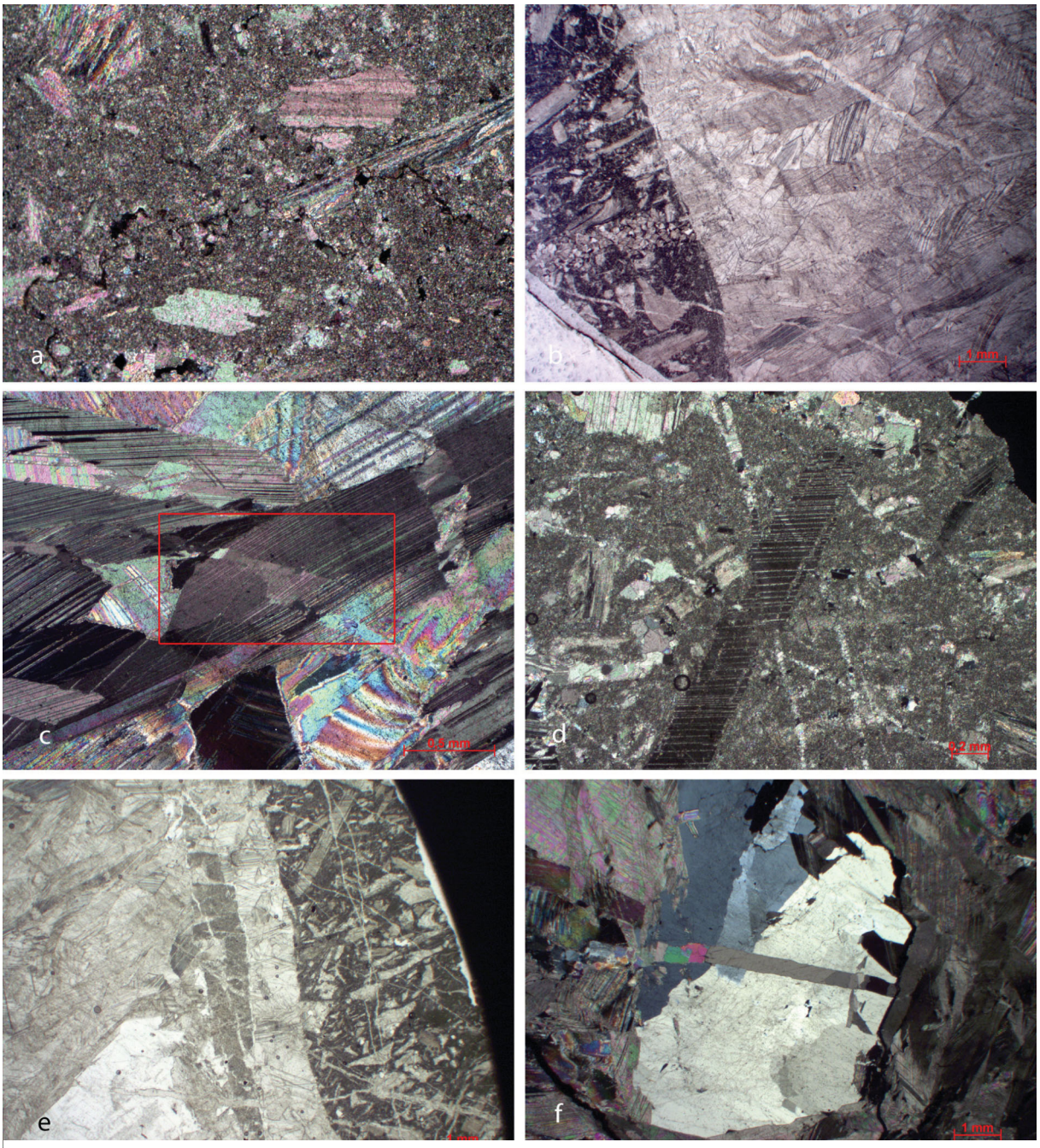

Fig. 42: Polarized images of thin section MA-2010-007. **a)** Stylolithes in host rock area. **b)** Microcrack crossing the HBV. **c)** Epitaxial grown microcrack. The calcite grains within the crack (red frame) show the same extinction as the surrounding material but different twinning characteristics. **d)** Primary structure crossed by epitaxial microcracks. **e)** Big fragment of host rock within vein area. **f)** Microcrack within quartz aggregate filled with calcite grains, which show less or no twinning.

The plug, which corresponds to this thin section, is not drilled into a specific predefined orientation. The drilling direction was angular from the side into the vein (cp. Fig. 43). The drilling linear is 018°/34°. The drilled vein is the same as that of the sample MA-2010-004 & 005. The thin section of this plug should be perpendicular to the vein. Therefore the plug is cut with 55° deviation from a perpendicular cut to the drilling linear. The final cut therefore has an orientation of 198°/21° (plane). The effective angle between cutting plane and vein is 75°, which is not exactly perpendicular to the vein.

This thin section includes host rock of both sides of the vein. The host rock area seen on the right side of the overview image (cp. A. 5) is approximately 50/50 of micritic and sparitic composition including primary structures such as fossils. Stylolithes are observable, as shown in Fig. 42a. Several microcracks are present, predominantly filled with calcite. The microcracks show a common orientation. In the thin section an angle of approximately 40° can be measured between the orientation of the microcracks and the HBV. It can not be definitely ascertained if this is the real angle between these structures or just an angled caused by this cut orientation. At one point a microcrack passes the HBV (cp. Fig. 42b), therefore this crack is formed posterior to the vein event. Other microcracks of the same orientation are present in the vein area as well. In this area the calcite grains within the microcrack show the same extinction as the surrounding calcite phase but they do not display the characteristic twinning (cp. Fig. 42c). Therefore these grains from within the microcrack grew epitaxial. Evidence of crack-seal are observable: host rock material is included in vein material.

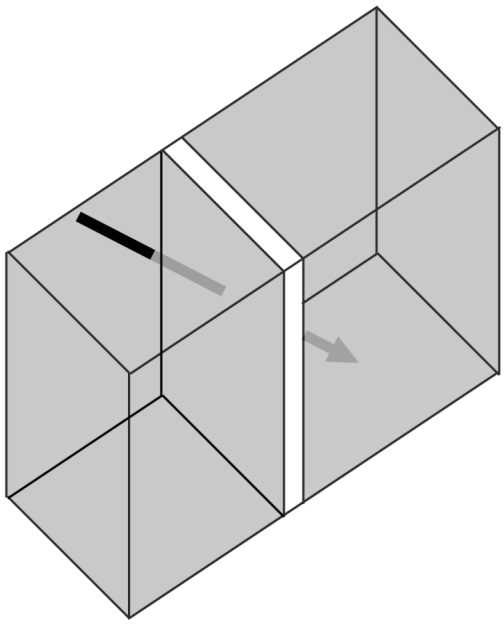

Fig. 43: Scheme illustrating the drilling orientation of MA-2010-007.

The second host rock area differs slightly from the host rock area previously discussed. The composition is predominantly micritic, including primary structures. Microcracks of the same orientation as the ones that are found in the first host rock area are observable once again. There, these cracks show clear evidence of epitaxial grain growth also within this host rock area (cp. Fig. 42d), which wasn't clearly detectable in the other host rock area. Additionally microcracks with an orientation parallel to the boundary between host rock and vein are present. A large part of host rock is found within the vein (cp. Fig. 42e), probably caused by a crack-seal process.

Generally the calcite phase displays twinning – both curved and straight – as already observed in the previously discussed thin sections. In addition to this, the quartz phase is present with previously observed characteristics such as undulose extinction, subgrains and fluid inclusions. Some of the fluid inclusions are oriented in bands. No clearly idiomorphic quartz grains were observed, thus the quartz phase appears to be xenomorphic. Some of the quartz aggregates show microcracks filled with calcite grains, which display less or no twinning (cp. Fig. 42f).

It is difficult to define homogeneous areas within the thin section. A small band of grains with shape preferred orientation, perpendicular to the boundary of host rock and vein, is noticeable at the host rock area situated in the right part of the overview image. Within the host rock area at the opposite site it is not that definite. However a trend of shape preferred orientation is also assumable, which is not perpendicular but angular to the boundary between host rock and vein. The trend of this growth direction is visible for many grains or aggregates. However nonetheless many more chaotic oriented areas within these 'oriented' areas make it impossible to clearly define a homogeneous area characterized by this noticeable trend of shape preferred orientation. In the central part of the vein area the grains are larger than close to the host rock areas.

3.4.5 MA-2010-008

The plug was drilled in z-orientation into an en echelon set. The vein is defined by 058°/75°, the orientation of the en echelon is 028°/80°. The drilling linear is defined by 005°/80°. Three thin sections are prepared from this plug. For two thin sections the plug was cut perpendicular to the drilling direction at different depths, these cuts have an orientation of 185°/10° (plane) respectively (MA-2010-008 a & b). For the third thin section, the plug was cut parallel to the drilling direction, effectively the cut is defined by the plane 258°/31°.

3.4.5.1 MA-2010-008a

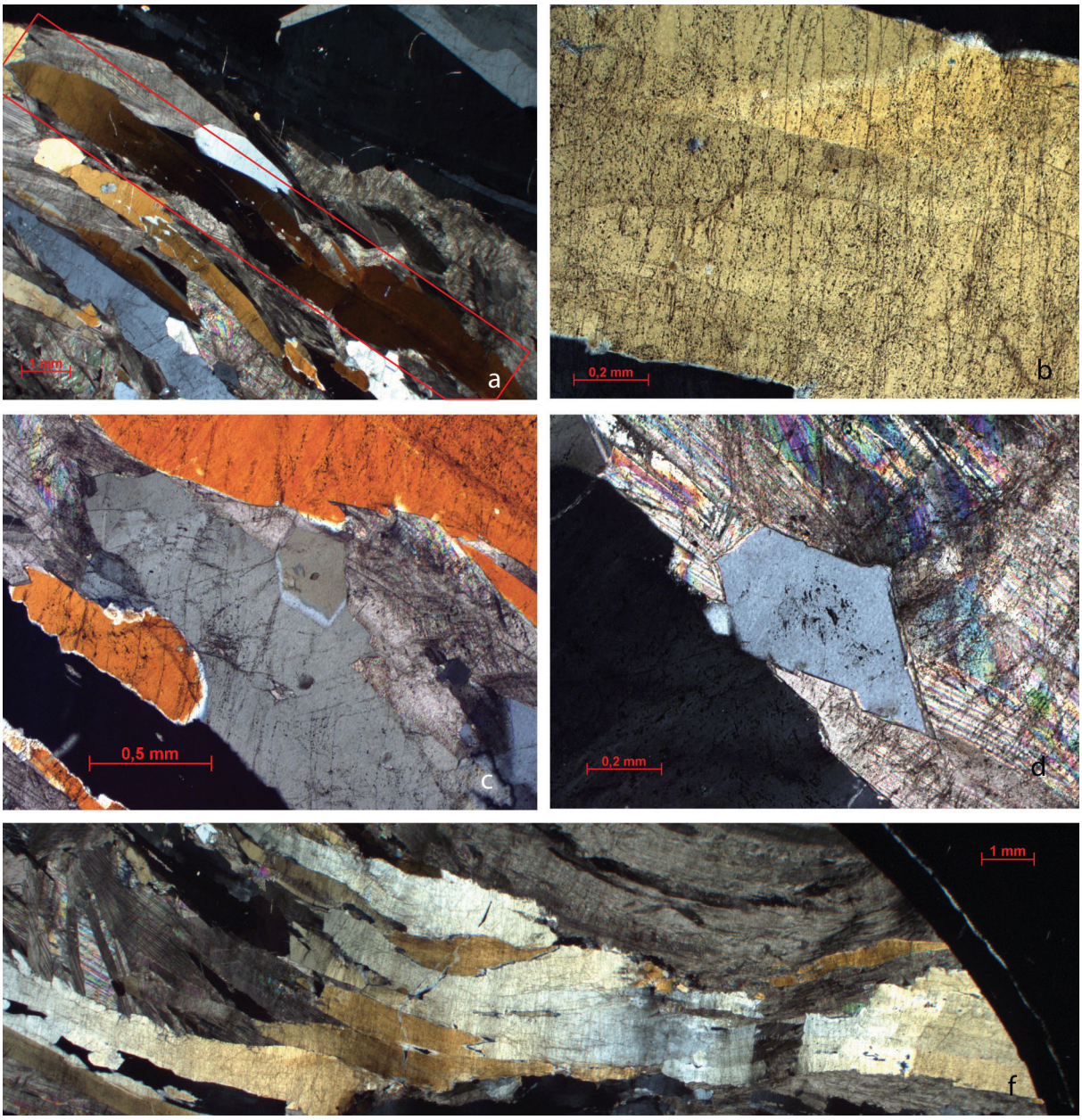

Fig. 44: Polarized images of thin section MA-2010-008a. **a)** Undulose extinction of elongated, fibrous quartz grains (highlighted with a red frame). **b)** Bands of fluid inclusion within quartz grain. **c)** Idiomorphic quartz grain. **d)** Hypidiomorphic quartz grain surrounded by calcite. **e)** A fibre seems to cross the 'separating band' and therefore changes the curving direction.

This thin section is prepared from the cut, which is the closest to bedding surface, therefore at lowest depth. Host rock is not observed within the thin section. Both phases, quartz and calcite, are present with a approximate 50/50 composition. The quartz fraction is obviously higher compared to previously discussed thin sections.

Generally twinning of calcite is observable consistently in the whole thin section. Fluid inclusions within calcite crystals are also present but more difficult to observe, compared to fluid inclusions within quartz grains due to optical effects caused by the high optical refraction of calcite. The calcite phase shows predominantly idiomorphic to hypidiomorphic grains.

The undulose extinction of the quartz grains is clearly visible in the thin section as shown in Fig. 44a. Subgrains are clearly visible in several quartz grains. A lot of fluid inclusion is observable, also arranged in bands with a preferred orientation: These oriented fluid inclusions are for example occurring at subgrain boundaries but are not restricted to these boundaries: the bands of fluid inclusions visible in Fig. 44b are not connectable to subgrain boundaries but maybe caused by microcracks.

Idiomorphic quartz grains are detectable in the thin section (cp. Fig. 44c) but also grains with a more hypidiomorphic grain shape as shown in Fig. 44d.

Characteristic of this thin section are the very elongate fibrous grains with a curved shape preferred orientation and homogeneous grain sizes. A type of band is visible in the central part of the thin section, dividing it into two parts. The band seems to be similar to an asymptote to the fibre's curved shape preferred orientations, whereby the sectors show different directions of curving (cp. Fig. 45). Both sectors nonetheless have to be regarded together, because they refer to the sinistral shear sense of the drilled en-echelon-system. The undulose extinction of the quartz grains argues for a straight growth of the grains followed by an event, which caused the retrospectively curving of these grains. It seems as if an observed fibre potentially passes the separating band and therefore also changes the direction of curving in this area (cp. Fig. 44e).

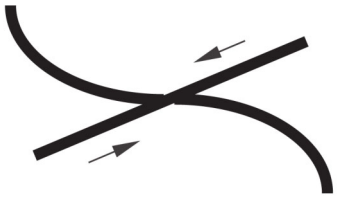

Fig. 45: Sketch illustrating the main configuration of the fibres

3.4.5.2 MA-2010-008b

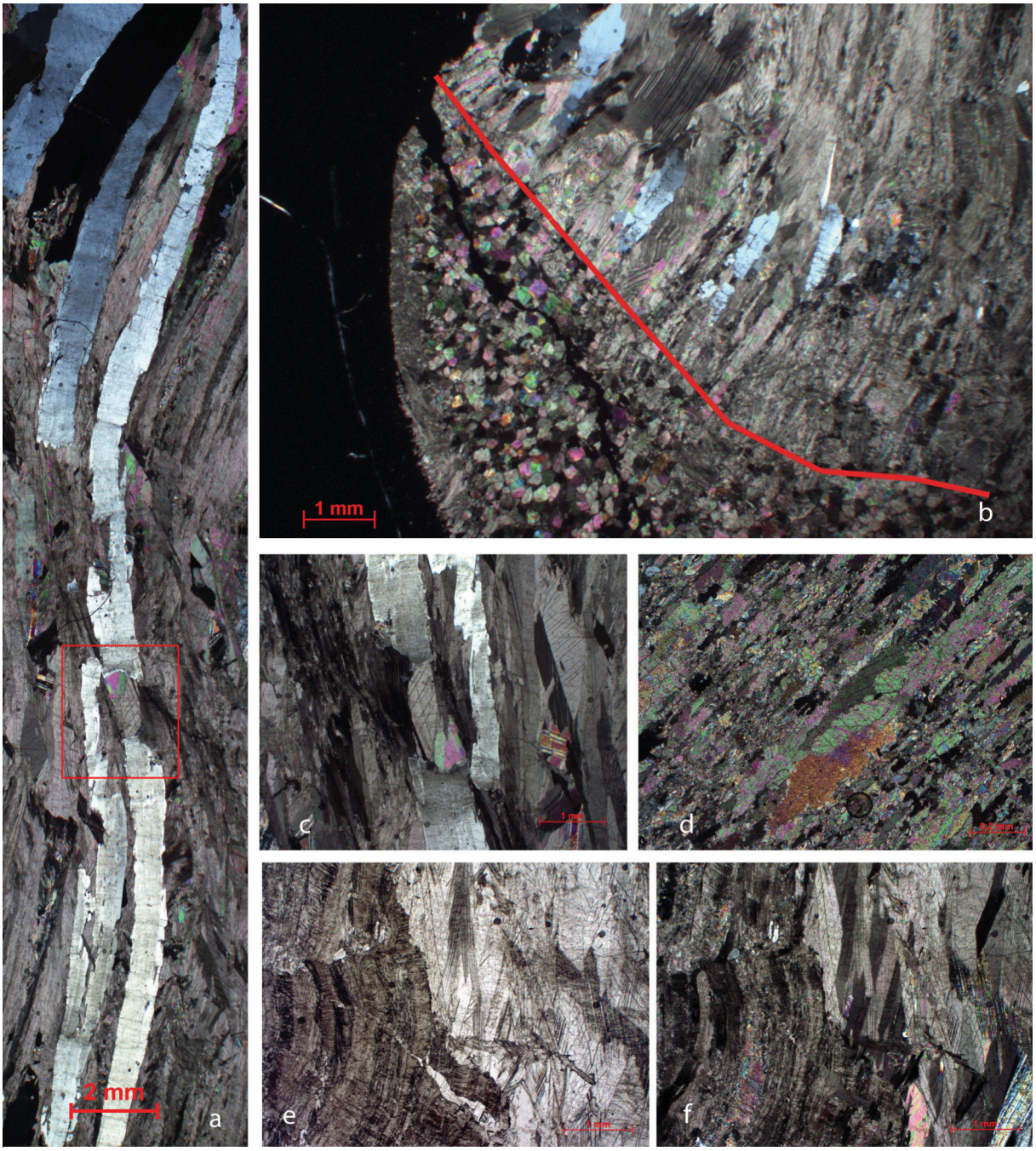

Fig. 46: Polarized images of thin section MA-2010-008b. **a)** A quartz fibre crosses the 'median band' and changes its curving direction. It covers in its length the entire thin section and is just interrupted by a single calcite grain (red frame), as is shown in **c). b)** Shape preferred orientation perpendicular to the HBV. A red line highlights the HBV. **d)** Area with calcite grains, which show less or no twinning. **e)** & **f)** chaotic area separated from a more definite area by a type of suture. Image with polarized light and without crossed niccols.

This thin section is the second one with a cut orientation perpendicular to drilling direction, even deeper below surface. Generally the calcite phase is present with twinning, often with an idiomorphic shape. Undulose extinction and subgrains are observed in the quartz phase. Fluid inclusions in quartz grains are detectable, also arranged in the form of bands with a principal direction. Clearly idiomorphic crystals were not observed, but several xenomorphic grains.

A small part of host rock extends into the vein area in the form of a ‘wing’ (cp. A. 7). This host rock part is of sparitic composition and has slightly curved but diffuse edges. At the inside part of the ‘wing’, a shape preferred orientation of small grains perpendicular to the HRV can be observed as visible in Fig. 46b (red line marks the HRV). Similarities to the previous thin section are visible. The identical opposed, curved, ‘asymptotic’ to a median line, shape preferred orientation as described already for the previous thin section is once again observable. The difference between both thin sections is, that in this case not the entire thin section follows this attribute and the grain sizes are much more heterogeneous. A curved quartz fibre – covering in its length the entire thin section - is observable, apparently it crosses the ‘median band’ and therefore changes its curving direction (Fig. 46a). It is only interrupted by a single calcite grain as shown in Fig. 46c. Another conspicuous, homogeneous area is characterized by relatively small calcite grains with a shape preferred orientation. This area shows calcite grains with less to no twinning (Fig. 46d).

A kind of suture separates a chaotic from a more definite area in respect to grain characteristics. In Fig. 46f, this becomes evident: At one side of the suture, single grains are well definable by their crystal planes and twinning is clearly visible. On the other side these characteristics can’t be observed clearly, it seems ‘messy’. The difference is also observable without crossed niccols in the form of colour differences (cp. Fig. 46e). The suture shows a triple junction, visible in both pictures with crossed and parallel niccols.

3.4.5.3 MA-2010-008c

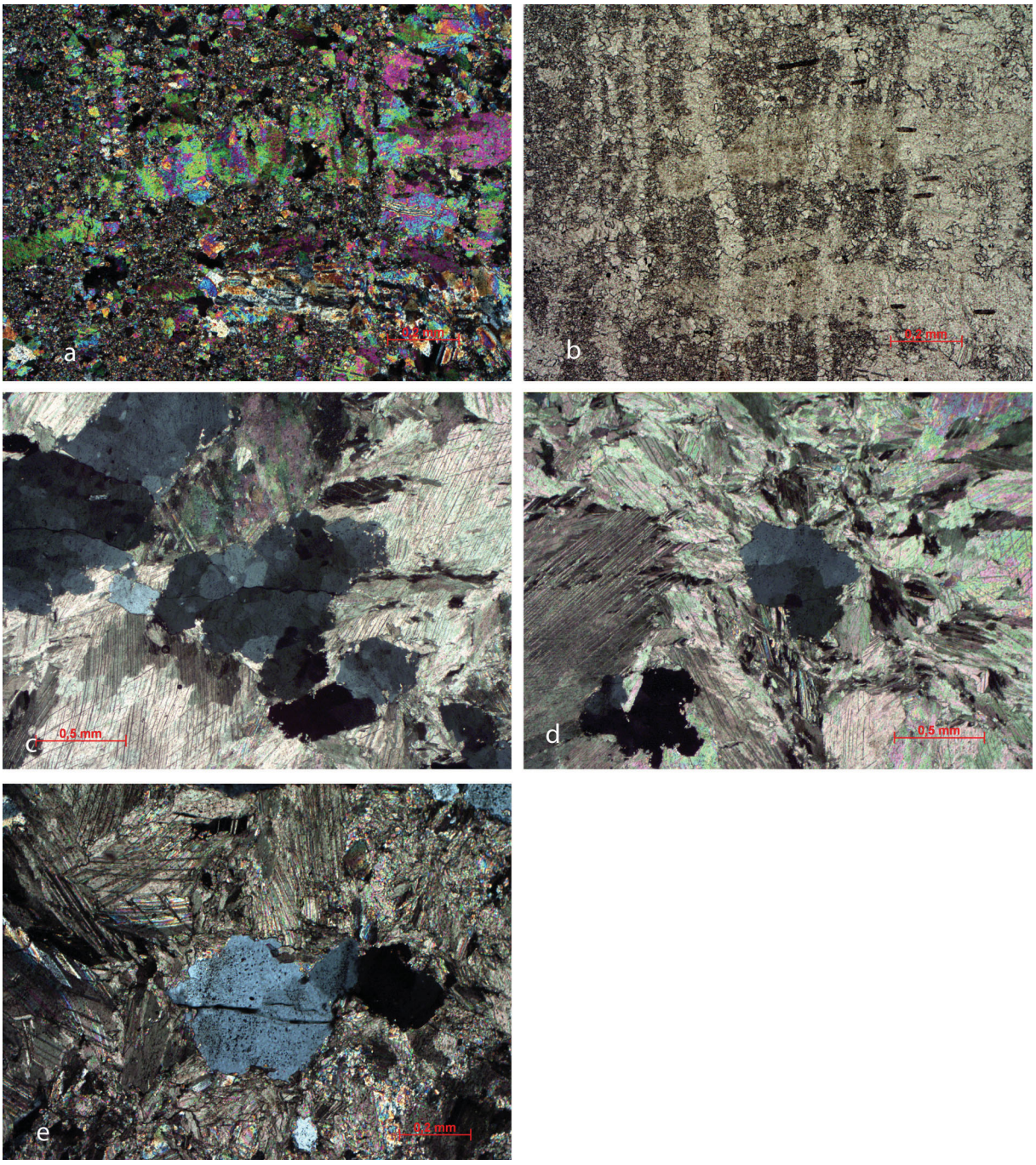

Fig. 47: Polarized images of thin section MA-2010-008b. **a)** & **b)** Several microcracks well visible without crossed niccols. The cracks cross primary structures. Under polarized light they are not (easy) to detect which could be a hint for epitaxial grain growth. **c)** Subgrains in quartz aggregates. **d)** Hypidiomorphic quartz grain. **e)** Quartz grain rudimentary showing crystal planes, which belong to the quartz lattice. This could be a hint for idiomorphic grain growth.

This thin section is prepared from the deepest section of the plug. Both phases, calcite and quartz are present with heterogeneous grain sizes. Large grain sizes are observed at the centre in the form of a band, in other parts grain size declines. Generally the calcite phase shows twinning but in many areas the grains seem to be 'washy', except in the central area. Idiomorphic calcite grains are found in the central part of the thin section. The quartz phase as in all previously discussed thin sections shows undulose extinction as well as subgrains (Fig. 47c) and fluid inclusions. Many hypidiomorphic quartz grains can be observed, as for example the one visible in Fig. 47d. Some of these grains have fragments of calcite included, this may indicate contemporaneous grain growth. Rarely observable are quartz grains, which show rudimentary crystal planes belonging to the quartz lattice (Fig. 47e). This could indicate idiomorphic grain growth.

Two areas of host rock are visible without crossed niccols. Both boundaries between host rock and vein are very diffuse and therefore not clearly definable. It is just possible to define an area where host rock is definitively present. The clearly identified part of host rock is of micritic composition including primary structures. Areas excluding this clear host rock area are of sparitic composition and also include primary structures, which is a hint that this area also can be titled as host rock material. Several microcracks are clearly visible without polarized light but not distinguishable by polarization colours from surrounding material under crossed niccols (Fig. 47a&b). This is a hint for epitaxial grain growth. Nonetheless an age relationship is possible; the cracked structure is a primary structure, i.e. a fossil. This also suggests that the area is still host rock area. The arrangement of many parallel microcracks - as the one described previously – can be caused by several crack-seal processes.

Most areas include predominantly blocky crystals with a more or less chaotic arrangement. In the central area a band of bigger grains have a trend to a shape preferred orientation but this is really not clear.

4 Acknowledgments

Thanks to …

… my supervisor Prof. Dr. Janos Urai for the opportunity of participating in this project and of realizing fieldwork in the Oman Mountains.

… Simon Virgo and Max Arndt for their guidance during the fieldwork, office-based work and preparation of the bachelor thesis. They helped with words and deeds, any time they tried to pass their knowledge. Last but not least I'm grateful for the great time in Oman.

… Sebastian Thronberens, Alexander Raith and Ben Laurich for the great time in the Oman Mountains. Their help was essential for the successful fieldwork.

… my girlfriend Stefanie Eppert for her patience during the preparation of my bachelor thesis. I know that for her the time was not always easy. She is there for me any time.

… to my family for supporting me. Without their help, my studies wouldn't be possible. I am especially grateful to my mother for supporting me in any situation.

… my uncle and aunt, Volker and Antonia Braun, for their language review of my thesis.

This study was carried out within the framework of DGMK (German Society for Petroleum and Coal Science and Technology) research project 718 "Mineral Vein Dynamics Modelling", which is funded by the companies ExxonMobil Production Deutschland GmbH, GDF SUEZ E&P Deutschland GmbH, RWE Dea AG and Wintershall Holding GmbH, within the basic research programme of the WEG Wirtschaftsverband Erdöl- und Erdgasgewinnung e.V. We thank the companies for their finacial support and their permission to publish these results.

5 Bibliography

Adobe. 2007. Photoshop CS3 Extended, San Jose, California, U.S., Adobe Systems.

AutopanoWiki. 2008. Interpolation and blenders. http://www.autopano.net/wiki-en/action/history/Interpolation_and_blenders, 30.9.2010.

AutopanoWiki. 2009a. Control Points Editor. http://www.autopano.net/wiki-en/action/view/Control_Points_Editor, 30.9.2010.

AutopanoWiki. 2009b. Render Settings. http://www.autopano.net/wiki-en/action/view/Render_Settings, 30.9.2010.

ESRI. 2004. ArcMap 9.3. In: ArcInfo Desktop 9.3. ESRI, Redlands, California, U.S.

Glennie, K.W. 1995. THE GEOLOGY OF THE OMAN MOUNTAINS An outline of their origin. *Scientific Press LTD, Beaconsfield.*

Holland, M., Urai, J. L., Muchez, P. & Willemse, J. M. 2009. Evolution of fractures in a highly dynamic thermal, hydraulic, and mechanical system; (I), Field observations in Mesozoic carbonates, Jabal Shams, Oman Mountains. *GeoArabia [Manama]* 14(1), 57-110.

Kolor. Autopano Giga 2. Kolor, Challes-les-Eaux, France.

Laurich, B. 2010. Multiscale analysis of the structural evolution of the southern flank of the Western Jabal Akhdar Anticline, Oman (vein examination, structural mapping and inverse remote sensing*). Master thesis, Geologie - Endogene Dynamik, RWTH Aachen University, Aachen*, not published.

Pratt, B. R., J. Smewing, D. 1993. Early Creataceous platform-margin configuration and evolution in the central Oman Mountains, Arabian Peninsula. *AAPG Memoir* 56, 201-212.

Raith, A. 2010. Creation of a high resolution panorama, capturing a high density calcite vein network from a polished limestone outcrop in the Oman Mountains. *Bachelor thesis, Geologie - Endogene Dynamik, RWTH Aachen University, Aachen*, not published.

Searle, M. P. 1985. Sequence of thrusting and origin of culminations in the northern and central Oman Mountains. *Journal of Structural Geology* 7-2, 129-143.

Thronberens, S. 2010. High resolution imaging of a large calcite vein network from a polished limestone outcrop in the Oman Mountains: Image acquisition, initial stereophotogrammetry and first interpretation. *Bachelor thesis, Geologie - Endogene Dynamik, RWTH Aachen University, Aachen*, not published.

Virgo, S., Arndt, M. 2010. Evolution of a crack-seal calcite vein network in limestone: a high resolution structural, microstructural and geochemical study from the Jebel Akhdar high pressure cell, Oman Mountains*. Diploma thesis, Geologie - Endogene Dynamik, RWTH Aachen University, Aachen, published in RWTH Aachen Hochschulbibliothek* (URN: urn:nbn:de:hbz:82-opus-33858).

6 Appendix

A. 1 **DVD**
Table of contents:

- Panorama data
    - Panorama images
    - Rectified detail images
    - Rectified microstructural images
    - Shapefiles
    - Reference grid
- Test renderings
    - Series 1
    - Series 4
- Full resolution microstructural images
- PDF version of the thesis
- Table with vein investigations

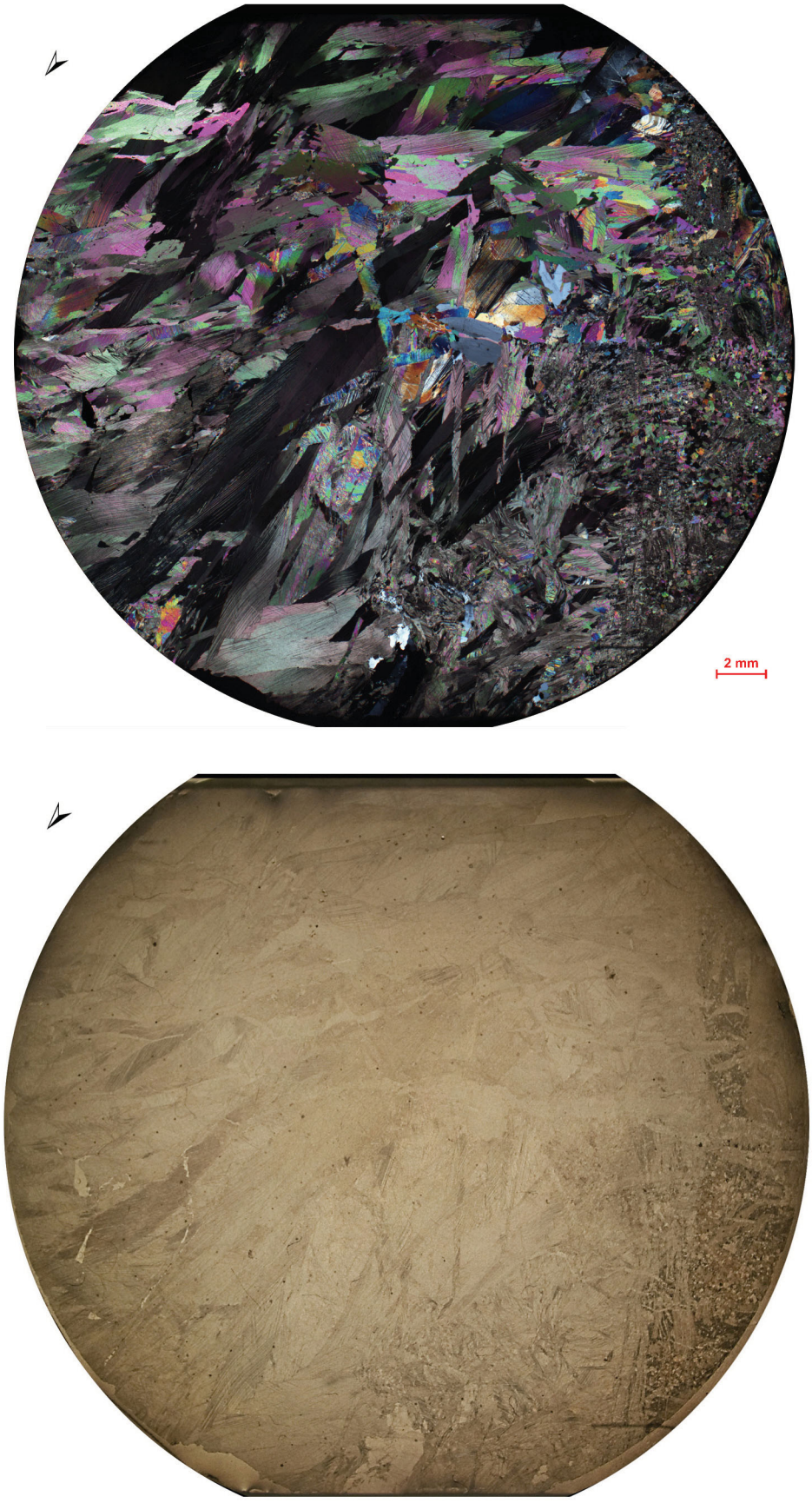

A. 2: Overview images of MA-2010-004 (polarized and without crossed niccols).

A. 3: Overview images of MA-2010-005 (polarized and without crossed niccols).

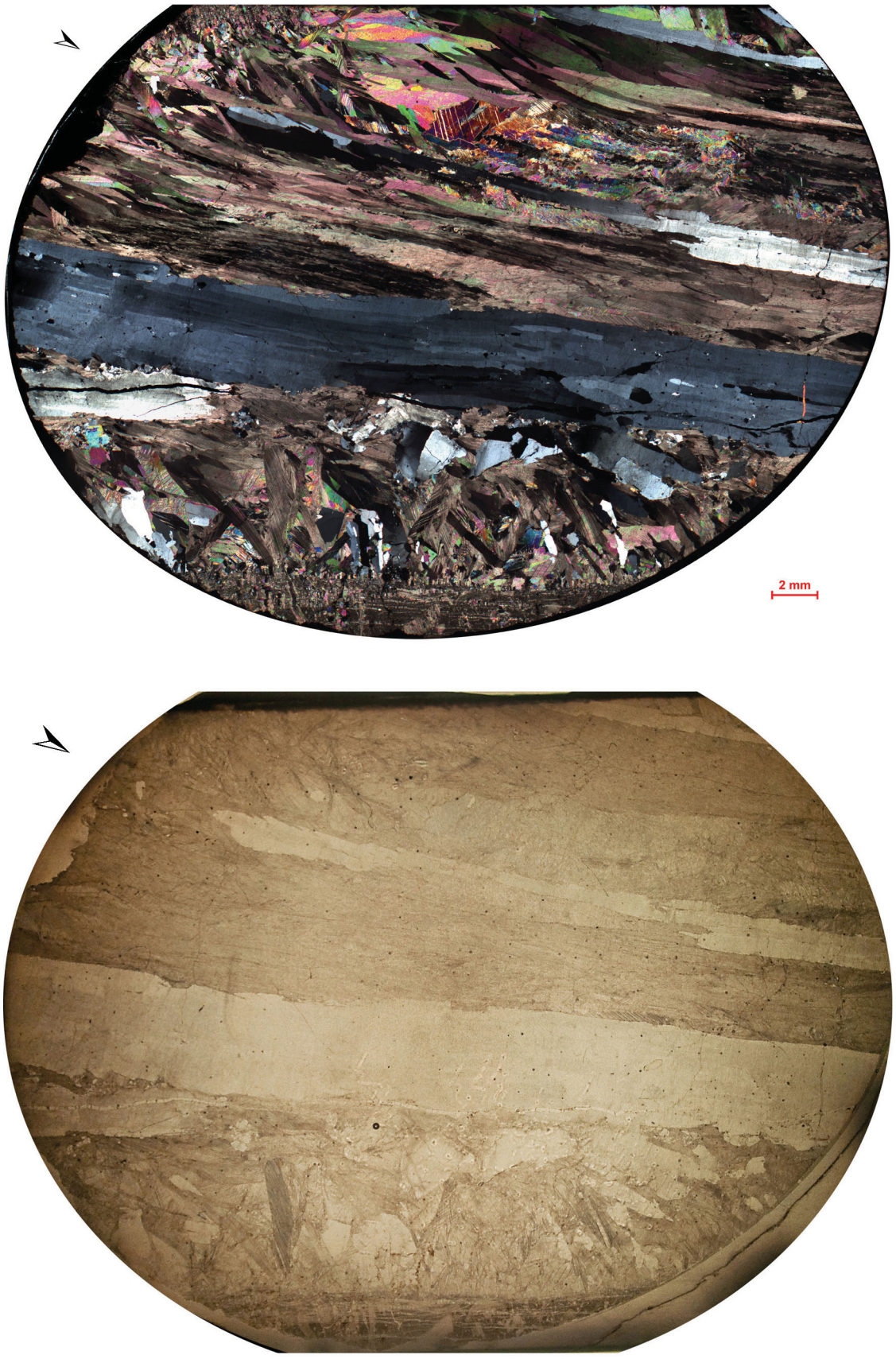

A. 4: Overview images of MA-2010-006 (polarized and without crossed niccols).

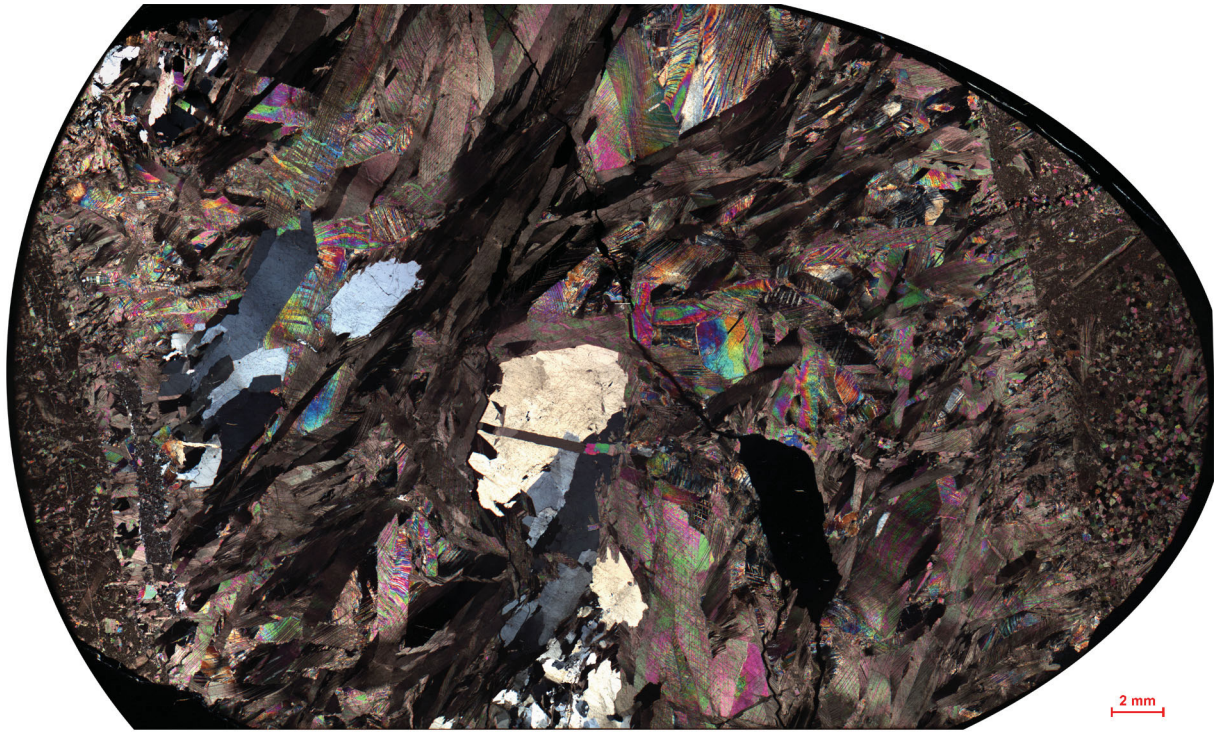

A. 5: Overview images of MA-2010-007 (polarized and without crossed niccols).

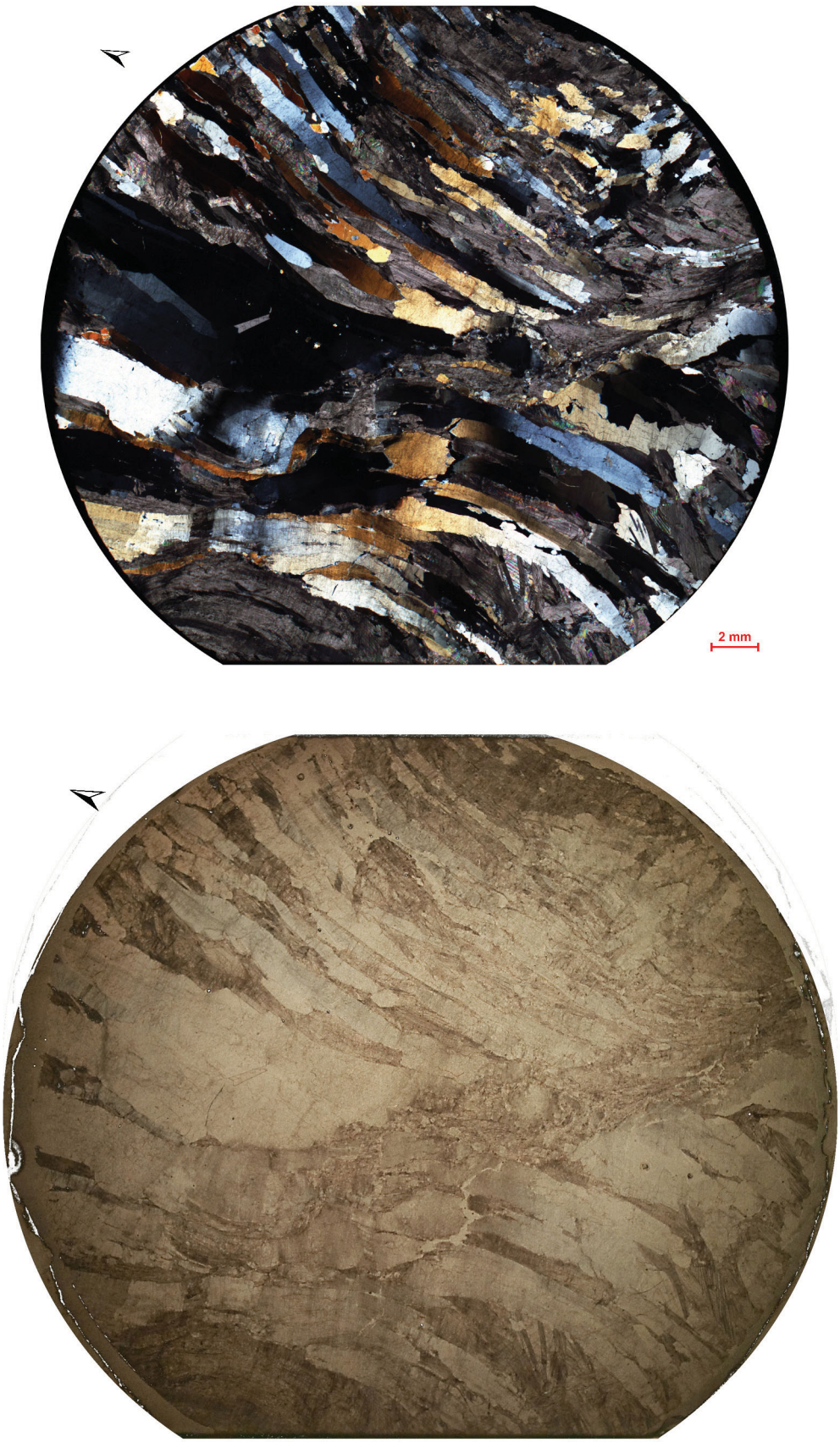

A. 6: Overview images of MA-2010-008a (polarized and without crossed niccols).

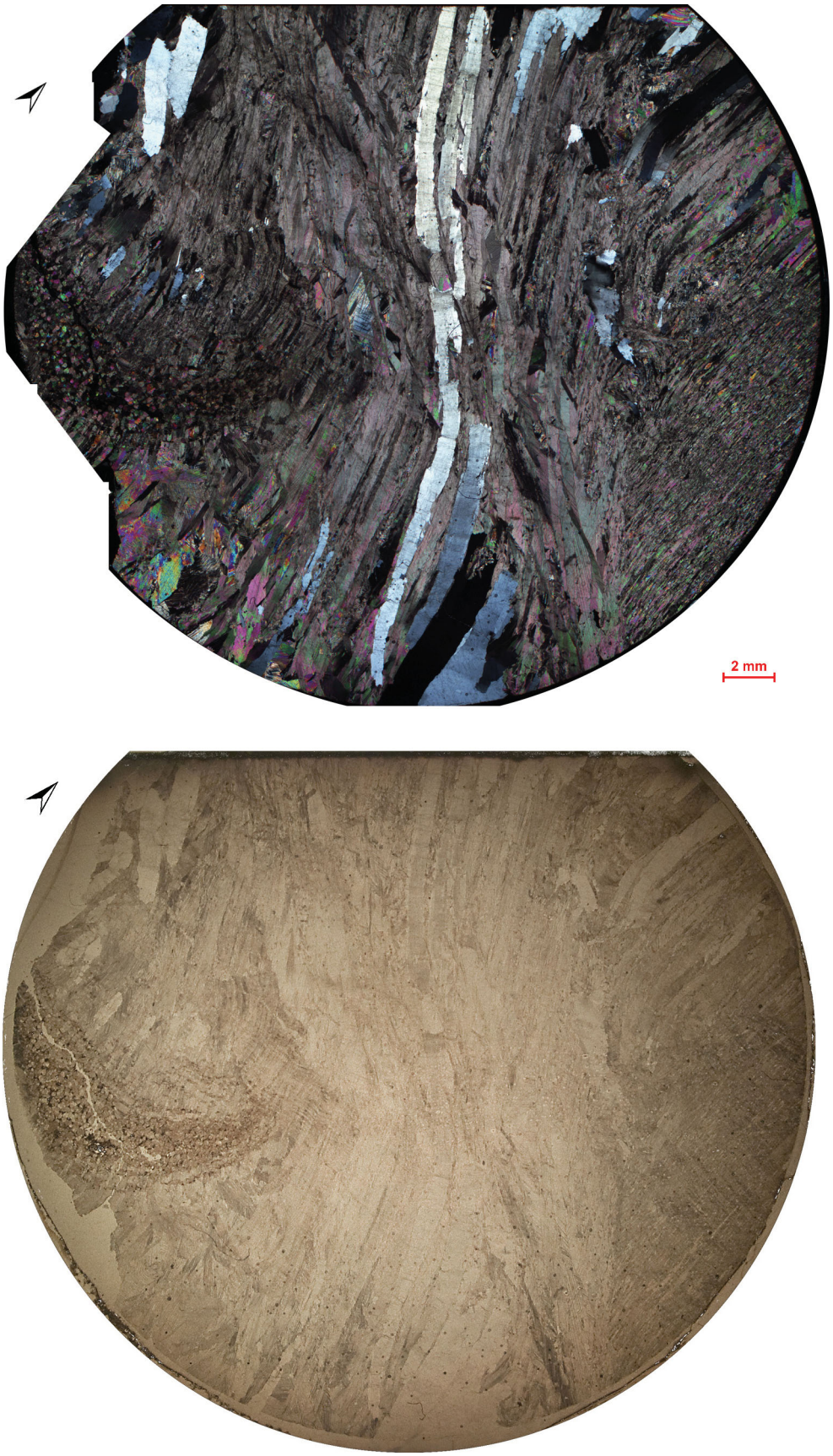

A. 7: Overview images of MA-2010-004b (polarized and without crossed niccols).

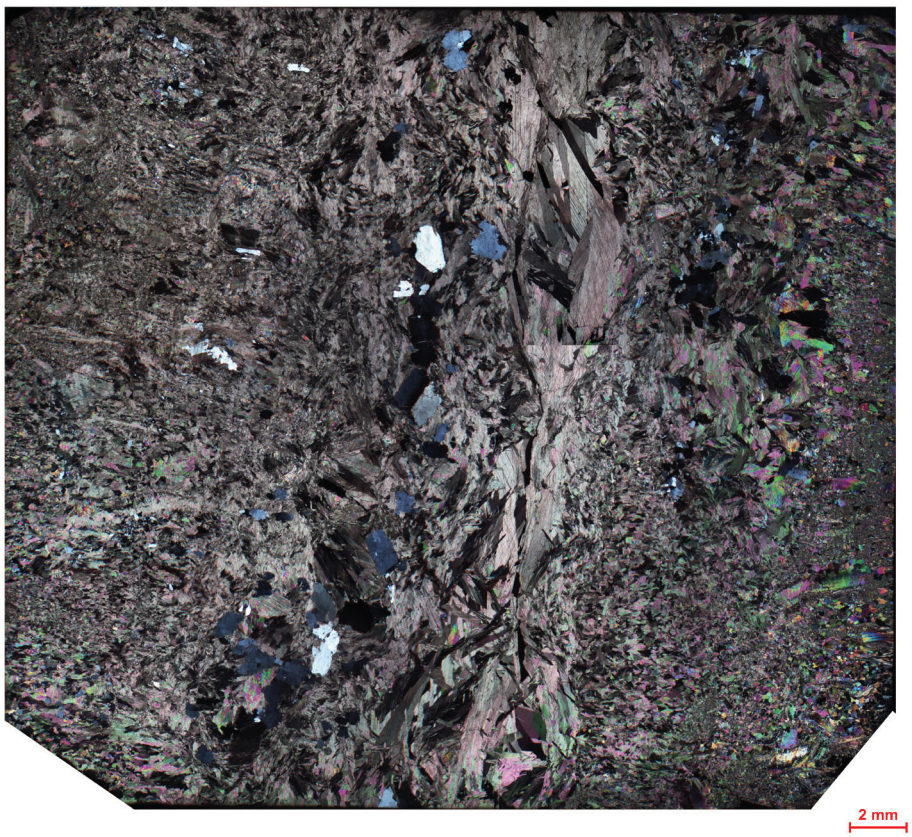

A. 8: Overview images of MA-2010-008c (polarized and without crossed niccols).

A. 9: Checklist for vein analysis.

Quadrant	The quadrant of the analyzed vein helps to identify the vein afterwards in the image
Layer	Having a look at the pavement it is obvious that one can identify 3 main layers in the pavement which are arranged like steps: • Layer 1: “Fibrous layer” • Layer 2: “En echelon layer” • Layer 3: “Bottom layer”
Orientation	As one can see some veins are exposed as 3D structure which makes it possible to measure precisely dip direction and dip, which is the favoured notation of the veins’ orientations. If this measurement is not possible at least the striking is noted. This striking is measured as a projection on a horizontal plane.
Aperture	The aperture is measured because it is considered to become interesting for further work on the images.
Habitus of calcite crystals in vein	This point of the checklist is one of the focuses of the detail work. The attributes are: • **Fibrousity,** if so including the orientation of the fibres. The exposed 3D structures again deliver the favoured measured data: dip direction and dip of the fibres. The alternative is the notation of the strike of the fibres, which is again the projection of the striking on a horizontal plane. • **Blocky,** no favoured growth direction macroscopically observable • **Not determinable**
Additional data	If observed, the following attributes are noted as well: • **tip splays** • **Wings** • **Stepover** • **Stylolites** in / crossing the / next to the calcite vein
Type of vein	• **Tabular** • **En echelon.** If so, the en echelon set is described by the orientation of the en echelons; whether they are lenticular or sigmoidal; dextral or sinistral • **Curved**

A. 10: Bedding measurements of the Swimming pool pavement.

Dip direction	Dip	Dip direction	Dip
220	10	229	10
220	8	219	7
227	10	239	10
224	10	214	6
205	5	233	15
210	7	215	10
Averaged values		221	9